Mon. Not. R. Astron. Soc. **000**, 1–?? (2005) Printed 23 January 2015 (MN LATEX style file v2.2)

Dust-regulated galaxy formation and evolution: A new chemodynamical model with live dust particles

Kenji Bekki[1⋆]
[1]*ICRAR M468 The University of Western Australia 35 Stirling Hwy, Crawley Western Australia 6009, Australia*

Accepted, Received 2005 February 20; in original form

ABSTRACT

Interstellar dust plays decisive roles in the conversion of neutral to molecular hydrogen (H_2), the thermodynamical evolution of interstellar medium (ISM), and the modification of spectral energy distributions (SEDs) of galaxies. These important roles of dust have not been self-consistently included in previous numerical simulations of galaxy formation and evolution. We have therefore developed a new model by which one can investigate whether and how galaxy formation and evolution can be influenced by dust-related physical processes such as photo-electric heating, H_2 formation on dust, and stellar radiation pressure on dust in detail. A novel point of the model is that different dust species in a galaxy are represented by 'live dust' particles (i.e., not test particles). Therefore, dust particles in a galaxy not only interact gravitationally with all four components of the galaxy (i.e., dark matter, stars, gas, and dust) but also are grown and destroyed through physical processes of ISM. First we describe a way to include dust-related physical processes in Nbody+hydrodynamical simulations of galaxy evolution in detail. Then we show some preliminary results of dust-regulated galaxy evolution. The preliminary results suggest that the evolution of dust distributions driven by radiation pressure of stars is very important for the evolution of star formation rates, chemical abundances, H_2 fractions, and gas distributions in galaxies.

Key words: ISM: dust, extinction – galaxies:ISM – galaxies:evolution – infrared:galaxies – stars:formation

1 INTRODUCTION

Galaxy formation is a complicated combination of many different physical processes, such as gravitational collapse (Eggen et al. 1962), accretion of subgalactic clumps (e.g., Searle & Zinn 1978), hierarchical merging of dark matter halos (e.g., White & Rees 1978), star formation and its feedback effects (e.g., Larson 1974; Dekel & Silk 1986), growth of bars and spiral arms (e.g., Sellwood & Carlberg 1984; Athanassoula 2003), clump dynamics (e.g., Noguchi 1999), feedback effects of active galactic nuclei (e.g., Di Matteo et al. 2005; Springel et al. 2005), hot and cold mode gaseous accretion (e.g., Keres et al. 2005; Dekel & Birmboim 2006), and environmental influences of groups and clusters (e.g., Dressler 1980; Bekki & Couch 2011). It has been a key issue for Galactic and extragalactic astronomy to understand the relative importance of each of these physical processes in the formation and evolution of galaxies with different masses and Hubble types residing in different environments at a give cosmic time. In order to address this key issue, many theoretical studies have tried to construct as realistic galaxy formation models as possible by using sophisticated numerical simulations.

One of the missing elements in these previous numerical studies of galaxy formation and evolution is interstellar dust. The efficient conversion from neutral to molecular hydrogen (H_2) is possible on the surface of dust grains (e.g., Gould & Salpeter 1963; Hollenbach & Salpeter 1971), and thermodynamical evolution of ISM and interstellar chemistry are also controlled by dust (e.g. Herbst 2002). Furthermore, fragmentation processes of metal-poor gas clouds can be significantly influenced by dust abundances so that dust can be very important for the formation of low-mass stars in the early universe (e.g., Larson 2005; Schneider & Omukai 2010). In spite of these importance of dust, dust-related physical processes have not been self-consistently included in almost all simulations of galaxy formation and evolution. The observed physical processes of dust properties in galaxies have been investigated so far by one-zone chemical evolution models (e.g., Dwek 1998, D98; Lisenfeld & Ferrara 1998; Hirashita 1999; Edmunds 2001; Inoue 2003; Calura et al. 2008; Asano

⋆ E-mail: bekki@cyllene.uwa.edu.au

et al. 2013; Zhukovska & Henning 2013; Rowlands et al. 2014).

Bekki (2013a, 2015; B13a and B15, respectively) have first performed numerical simulations of galaxy formation and evolution which include self-consistently both (i) the formation, growth, and destruction processes of dust grains in asymptotic giant branch (AGB) stars, supernovae (SNe), and ISM and (ii) H_2 formation on dust grains. Thanks to the self-consistent modeling of dust physics, not only the cosmic evolution of dust but also the physical properties of galaxies (e.g., gas contents) were compared with the latest observations (e.g., by Herschel) in B13a and B15. These simulations are different from previous ones (Ferrara et al. 1991, F91; Aguirre et al. 2001) in which dust grains are represented by 'test particles' (i.e., moving in a gravitational potential of a galaxy without influencing its host galaxy at all) so that the influences of dust on galaxy formation and evolution can not be investigated. Although our previous simulations made it possible for us to predict the cosmic evolution histories of dust abundances and distributions in galaxies, they have some problems in modeling dust.

One key problem is that gas and dust are assumed to move exactly the same way in our previous simulations (B13a, B15): the simulated spatial distributions and kinematics are the same between gas and dust in galaxies. This could be a good approximation, given that the timescale of gas-dust frictional timescale is an order of $\sim 10^3$ yr for a typical range of ISM properties (e.g., Theis & Orlova 2004), which is much shorter than the dynamical timescales of most galaxies ($10^7 - 10^8$ yr). However, as shown in previous theoretical works on dust evolution in galaxies, only dust can be expelled from galactic disks through the effects of radiation pressure of stars on dust (e.g., F91). Also, the observed flat distribution of halo dust (Ménard et al. 2010, M10) and the rather high dust-to-gas-ratio ($D \sim 0.05$) in M81 group (e.g., Xilouris et al. 2006) strongly suggest that the spatial distributions of dust can be quite different from those of gas in some galaxy environments.

Furthermore, chemical evolution of galaxies can be significantly influenced by dust removal from galaxies through radiation-driven winds (Bekki & Tsujimoto 2014), which implies that star formation processes in galaxies can be influenced by dust removal from galaxies owing to the processes dependent on dust and metal abundances. Therefore, we would need to model dust removal processes in galaxies more self-consistently so that we can discuss the roles of dust in galaxy formation and evolution and the observed wide variety of dust properties of galaxies in a more comprehensive way. It would be a reasonable strategy for numerical studies of galaxy formation to treat gas and dust separately, because gas and dust respond differently to physical processes of ISM.

The purpose of this paper is to describe a new method by which dust-related physics can be more self-consistently included in Nbody/hydrodynamical simulations of galaxy formation and evolution. Dust and gas are represented by separate 'live' particles in the present new simulation code so that dust-related physical processes such as radiation pressure on dust and dust-gas interaction can be better investigated. Since this is the very first paper discussing the possible roles of dust in galaxy formation based on a new type of galaxy evolution simulations, we focus mainly on the methods to include dust-related physics in Nbody/hydrodynamical simulations. We briefly describe some key results of the new simulations, and we discuss extensively the possible roles of dust in galaxy formation and evolution in forthcoming papers.

The present model is not only a more sophisticated version of previous models on the formation of dust wind (e.g., Chiao & Wickamasinghe 1972; F91) but also an improved version of previous galaxy evolution models for dusty galaxies. The important influences of radiation-driven dust wind on star-forming regions in galaxies have been recently discussed by a number of authors (e.g., Thompson et al. 2005; Hopkins et al 2012). These works, however, did not investigate the evolution of dust contents and the possibly separate distributions of gas and stars in a self-consistent manner. Furthermore, previous models for spectral energy distributions (SED) of galaxies (e.g., Bekki & Shioya 2000; Jonsson 2006) and for H_2 contents of galaxies (e.g., Pelupessy et al. 2006; Krumholz et al. 2009) assumed a fixed dust-to-metal (D_z) ratio across the entire region of a simulated galaxy. Such a fixed D_z is neither observed (e.g., Galametz et al. 2011) nor realistic in theoretical modeling of dust evolution (e.g., Inoue 2003). Therefore, the present model with variable D_z in different local regions of a simulated galaxy can provide more detailed and accurate predictions on H_2 contents and SEDs of galaxies.

The plan of the paper is as follows. First, we describe the details of the adopted new methods to implement dust-related physical processes in galaxy-scale chemodynamical simulations. Then, we present some key results of the new simulations on the roles of dust in the evolution of star formation rates, dust distributions, and gas dynamics within galaxies in §3. In this section, we also discuss how the present results depend on the physical parameters of the adopted new method for dust-related physics. In §4, we discuss (i) the advantages and disadvantages of the present new method over previous ones and (ii) further improvement of the method in our future works. We summarize our conclusions in §5.

Although including dust-related physics in galaxy-scale Nbody+hydrodynamical simulations is rather new in numerical studies of galaxy formation and evolution, there are already a number of more sophisticated simulations on the joint evolution of dust and gas in other areas of astronomy. For example, Laibe & Price (2014) have already included the gas-dust interaction for multiple dust components in their SPH simulations that can be used for the investigation of planet formation and evolution. The methods and numerical techniques used in these simulations in other areas of astronomy would be useful in the present study. However, we do not discuss these, because this is beyond the scope of this paper. We accordingly focus on the modeling issues of galaxy-scale chemodynamical simulations with dust physics.

2 THE MODEL

2.1 A new four-component galaxy model

The most remarkable difference in dust modeling between B13a and the present study is that gas and dust in ISM of galaxies are represented by separate 'live' particles. Accordingly, a galaxy consists of dark matter, stars, gas, and

Table 1. A list of physical processes implemented in the simulations codes used in B13a and this work. This table accordingly shows a number key differences between the two codes.

Physical effects	B13a [a]	This work	Specifications
Dust formation	◯	◯	Formation in SNe and AGB stars
Dust destruction	◯	◯	Destruction by SNe
Dust shattering in halo gas	×	×	
Dust coagulation	×	×	
Dust growth	◯	◯	Variable dust accretion timescale in this work
Size evolution of dust	×	×	
Size-dependence on dust composition	×	◯	Only two components (silicate and graphite)
Stellar radiation pressure on dust	×	◯	
Gas-dust hydrodynamical coupling	×	◯	
Photo-electric heating	×	◯	
Gas-dust heating	×	◯	
Cosmic-ray heating	×	◯	
UV background radiation	×	×	
H_2 formation on dust grains	◯	◯	
H_2 formation efficiency dependent on D and $ISRF$	◯	◯	
H_2 photo-dissociation by ISRF	◯	◯	ISRF locally defined for each gas particle
Star formation	◯	◯	H_2-dependent recipe
SN feedback effects	◯	◯	Both SNII and prompt SNIa are included.
AGN feedback effects	×	×	
Growth of SMBHs	×	×	
Chemical evolution	◯	×	11 elements (e.g., C, N, and O)
Chemical enrichment by AGB ejecta	◯	◯	
Dust-corrected cooling	◯	◯	[Fe/H] corrected by dust depletion is used.
Metallicity-dependent radiative cooling	◯	◯	For $T_g > 10^4$ K
[CII] + [OI] cooling	×	◯	Different cooling rate adopted in B13a
H_2 cooling	×	◯	For $T_g > 10$ K

[a] ◯ and × in the second column mean inclusion and non-inclusion of the listed physical effect, respectively

dust ('four-component' model) in the present study, which is different from almost all previous simulations of galaxy formation and evolution in which a galaxy consists of dark matter, gas, and stars ('three-component'). Dust particles gravitationally interact both with other components of galaxies (e.g. dark matter and stars) and with other dust particles in the new four-component model. Furthermore, gas-dust interaction and response of dust to radiation fields of stars can be more self-consistently included in the four-component model. As in B13a, H_2 formation on dust grains and the formation, growth, and destruction processes of dust due to star formation and SN feedback effects are included in the present model. By using an isolated disk galaxy model described in this section, we mainly discuss how radiation pressure of stars on dust grains can influence H_2 formation processes and star formation histories of galaxies.

The isolated disk model adopted in this study is the same as those in Bekki (2014b) and therefore we briefly describe it here. The models for H_2 formation on dust grains and the formation, growth, and destruction processes of dust in ISM of galaxies are essentially the same as those adopted in B13a. We thus describe the details of the models only when they are differently implemented in the present new simulations with live dust particles. Some new ingredients that were not included in B13a are described and discussed in detail in this section. Dust-related physical processes that are missing in the present model yet could be important in ISM evolution are discussed later in §4.

The new simulation code used in this work is based on the one developed in our previous works (B13a, B15) that can be run on clusters of GPU (Graphics Processing Unit) machines. In the new code, gravitational calculations of many particles can be done on GPUs whereas other calculations (e.g., star formation and hydrodynamics) can be done on CPUs. The GPUs are used also in calculating the radiative force (due to radiation pressure of a star particle on a dust particle) which is proportional to $L_{\rm star}/r^2$, where $L_{\rm star}$ is the total stellar luminosity and r is the distance between the dust and star particles. The code adopts the smoothed-particle hydrodynamics (SPH) method for following the time evolution of gas dynamics in galaxies. The key differences in the adopted models between B13a and this work are summarized in Table 1 and the physical meanings for symbols used in this work are given in Table 2.

2.2 Disk galaxy model

In the present disk model, a galaxy consists of dark matter, stars, gas, and dust: this is the 'four-component' disk model as opposed to the 'three-component' (i.e., dark matter + stars + gas) one adopted in almost all previous simulations of galaxy evolution. The total masses of dark matter halo, stellar disk, gas disk, bulge, and dust of a disk galaxy are denoted as $M_{\rm h}$, $M_{\rm s}$, $M_{\rm g}$, $M_{\rm b}$, and $M_{\rm dust}$, respectively. In order to describe the initial density profile of dark matter halo in a disk galaxy, we adopt the density distribution of the NFW halo (Navarro, Frenk & White 1996) suggested from CDM simulations:

$$\rho(r) = \frac{\rho_0}{(r/r_{\rm s})(1+r/r_{\rm s})^2}, \quad (1)$$

where r, ρ_0, and $r_{\rm s}$ are the spherical radius, the characteristic density of a dark halo, and the scale length of the halo, respectively. The c-parameter ($c = r_{\rm vir}/r_{\rm s}$, where $r_{\rm vir}$ is the virial radius of a dark matter halo) and $r_{\rm vir}$ are chosen appropriately for a given dark halo mass ($M_{\rm dm}$) by using the $c - M_{\rm h}$ relation predicted by recent cosmological simulations (e.g., Neto et al. 2007).

The bulge of a disk galaxy has a size of $R_{\rm b}$ and a scale-length of $R_{0,\rm b}$ and is represented by the Hernquist density profile. The bulge is assumed to have isotropic velocity dispersion and the radial velocity dispersion is given according to the Jeans equation for a spherical system. The radial (R) and vertical (Z) density profiles of the stellar disk are assumed to be proportional to $\exp(-R/R_0)$ with scale length $R_0 = 0.2R_{\rm s}$ and to ${\rm sech}^2(Z/Z_0)$ with scale length $Z_0 = 0.04R_{\rm s}$, respectively. The gas disk with a size $R_{\rm g} = 2R_{\rm s}$ has the radial and vertical scale lengths of $0.2R_{\rm g}$ and $0.02R_{\rm g}$, respectively. In addition to the rotational velocity caused by the gravitational field of disk, bulge, and dark halo components, the initial radial and azimuthal velocity dispersions are assigned to the disc component according to the epicyclic theory with Toomre's parameter $Q = 1.5$. The vertical velocity dispersion at a given radius is set to be 0.5 times as large as the radial velocity dispersion at that point.

2.3 Live dust particle

The initial distribution of dust and kinematics in a disk galaxy are assumed to be the same as those of the gas. The 'dust disk' of a galaxy is represented by live dust particles with the total particle number of $N_{\rm dust}$: this $N_{\rm dust}$ can increase according to the star formation history of the galaxy. The evolution of each dust particle can be influenced by (i) gravitational force from other components (e.g., stars) and other dust particles ($F_{\rm grav}$), (ii) radiation pressure of stars ($F_{\rm rad}$), and (iii) drag effects of surrounding gas particles ($F_{\rm drag}$). Thus, the total force exerting on the i-th dust particle is as follows:

$$F_i = F_{{\rm grav},i} + F_{{\rm rad},i} + F_{{\rm drag},i}. \quad (2)$$

The dust particles can be destroyed by SNe so that their masses ($m_{\rm d}$) can be drastically reduced when star formation occurs around the particles. It should be noted here that this dust particle mass ($m_{\rm d}$) is different from dust grain mass ($m_{\rm dust}$) for each dust component (silicate or graphite), which is later used. The dust particle is assumed to consist of numerous dust grains (e.g., silicate and graphite), and accordingly, $m_{\rm d} = \eta_{\rm dust} m_{\rm dust}$, where $\eta_{\rm dust}$ corresponds to the number of dust grains in a dust particle.

Since gas and dust move independently from each other in the present simulations, the spatial distributions of gas and dust in a galaxy can be different. Therefore, we estimate the H_2 formation on dust grains at each dust particle's position at each time step. This is quite different from B13a in which H_2 formation is estimated at each gas particle's position owing to the adopted assumption that gas and dust always have the same spatial distribution. The growth and destruction processes of dust are also estimated at each dust particle's position accordingly to the physical properties of gas around the dust particle. The detailed methods to implement these are described later in this section. The dependence of the present results on $N_{\rm dust}$ is briefly discussed in Appendix A.

Table 2. Description of physical meanings for symbols often used in the present study.

Symbol	Physical meaning
RP	Radiation pressure of stars on dust grains
PEH	Photo-electric heating of gas by dust
GD	Gas-dust heating of ISM
CR	Cosmic-ray heating of ISM
DR	Gaseous drag of dust
D	dust-to-gas ratio
$f_{\rm H_2}$	mass fraction of molecular hydrogen (H_2)
$Q^*_{\rm pr}$	Frequency-averaged radiation pressure coefficient
$A_{\rm t}$	Total dust extinction (mag)
t_0	Initial ages of stars in a disk
$f_{\rm dest}$	The mass fraction dust destroyed by SNe

2.4 Gravitational dynamics and hydrodynamics

Since the total number of particles (N) used in this study is an order of 10^6, we adopt a direct-summation N-body algorithm for gravitational interaction between dark matter, stars, gas, and dust. The calculation speed of the direct summation method can be significantly increased by using GPUs or GRAPE-DR, which is the latest version of the special-purpose computer for gravitational dynamics. In the present code, the gravitational softening length (ϵ) is chosen for each component in a galaxy (i.e., multiple gravitational softening lengths). Thus the gravitational softening length (ϵ) *can be* different between dark matter ($\epsilon_{\rm dm}$), stars ($\epsilon_{\rm s}$), gas ($\epsilon_{\rm g}$), and dust ($\epsilon_{\rm d}$), and ϵ is determined by the initial mean separation of each component.

The gravitational softening lengths for stars, gas, new stars, and dust are set to be the same with one another. Initial $\epsilon_{\rm g}$ is set to be significantly smaller than $\epsilon_{\rm dm}$ owing to rather high number-density of gas particles. Furthermore, when two different components interact gravitationally, the mean softening length for the two components is applied for the gravitational calculation. For example, $\epsilon = (\epsilon_{\rm dm} + \epsilon_{\rm g})/2$ is used for gravitational interaction between gas and dark matter. The values of $\epsilon_{\rm dm}$ and $\epsilon_{\rm g}$ ($= \epsilon_{\rm s}$) are 2.1 kpc and 0.2 kpc, respectively, for the fiducial MW-type disk model later described. Thus, the gravitational softening length for interaction between ith and jth particles is as follows:

$$\epsilon_{i,j} = \frac{\epsilon_i + \epsilon_j}{2}, \quad (3)$$

where ϵ_i and ϵ_j take either of the above five (virtually two) values for the five components.

We consider that galactic ISM composed of gas and dust can be modeled as an ideal gas with the ratio of specific heats (γ) being 5/3. The gaseous temperature ($T_{\rm g}$) is set to be 10^4 K initially in all models. The basic methods to implement SPH in the present study are essentially the same as those proposed by Hernquist & Katz (1989). We adopt the predictor-corrector algorithm (that is accurate to second order in time and space) in order to integrate the equations describing the time evolution of a system. Each particle is allocated an individual time step width (Δt) that is determined by physical properties of the particle. The maximum time step width ($\Delta t_{\rm max}$) is 0.01 in simulation units, which means

that $\Delta t_{\rm max} = 1.41 \times 10^6$ yr in the present study. Star formation rates, chemical abundances, H_2 fractions, and dust properties are all updated once for every $\Delta t_{\rm max}$.

The radiative cooling processes for $T_{\rm g} > 10^4$K are properly included by using the cooling curve by the MAPPINGS III code (Sutherland & Dopita 1993). It should be stressed here that in estimating the cooling rate depending on gas-phase metallicity and temperature, we use the correct gas-phase metallicity for each gas gas particle. Here 'correct' means that dust-phase metals (i.e., those locked up into dust grains thus can not participate radiative cooling) are excluded from the estimation of gas-phase metallicities. In estimating gas-phase [Fe/H] in B13a and B15, we calculate the gas-phase Fe mass ($m_{\rm Fe,g}$) for each particle at each time step as follows:

$$m_{\rm Fe,g} = m_{\rm Fe,t} - m_{\rm Fe,d}, \quad (4)$$

where $m_{\rm Fe,t}$ and $m_{\rm Fe,d}$ are the total Fe mass and Fe mass locked up in dust for the particle. In the present model, we can simply use the total Fe mass of a gas particle as $m_{\rm Fe,g}$, because the evolution of gas and that of dust are separately examined at each time step (i.e., $m_{\rm Fe,d}$ is always 0 for gas). Thus, the present simulation can better estimate the cooling rates for gas particles than previous simulations that do not include dust.

For $10 \leqslant T_{\rm g} \leqslant 10^4$K, we adopt two analytic formulae proposed by Wolfire et al. (2003) for gas cooling in neutral atomic regions (e.g., by [CII] 158μm cooling) and by Galli & Palla (1998) for H_2 cooling. The cooling rate coefficient by Wolfire et al. (2003) is as follows:

$$\Lambda_{\rm CII+OI} = 5.4 \times 10^{-27} T_2^{0.2} e^{-1.5/T_2} Z_{\rm g}^{'} \ {\rm ergs\ cm^3\ s^{-1}}, \quad (5)$$

where $T_2 = T_{\rm g}/100$ ($T_{\rm g}$ is the gas temperature in units of K) and $Z_{\rm g}^{'}$ is the gas-phase metallicity normalized by the solar value (0.02). Since this cooling rate is per $n_{\rm H}^2$ (where $n_{\rm H}$ is the hydrogen number density), $n_{\rm H}$ needs to be calculated for each SPH particle at each time step for estimating the cooling rate. The above adopted formula is an approximation that Wolfire et al. (2003) derived from full numerical calculations of ISM by assuming that H atoms are responsible for the excitation of [CII] and [OI] for the gas density less than 3000 cm^{-3} and the gas temperature ranging from 100 K to 1000 K.

We adopt the equation A7 described in Galli & Palla (1998) for H_2 cooling and the formula is as follows:

$$\log \Lambda_{\rm H_2} = -103.0 + 97.59 \log T_{\rm g} - 48.05 (\log T_{\rm g})^2 + 10.80 (\log T_{\rm g})^3 - 0.9032 (\log T_{\rm g})^4. \quad (6)$$

Since this cooling rate is per $n_{\rm H} n_{\rm H_2}$, we need to calculate the hydrogen number density ($n_{\rm H}$) and H_2 number density ($n_{\rm H_2}$) of a SPH gas particle in order to estimate the H_2 cooling rate for the particle. In the above H_2 cooling formula, galaxies with higher dust abundances are likely to show more efficient H_2 cooling, because H_2 formation rates are higher in such galaxies. Therefore, thermal evolution of ISM and thus gas dynamics of galaxies can be significantly influenced by dust evolution in the present study.

As shown in Galli & Palla (1998) and Hollenbach & McKee (1989), this H_2 cooling rate depends on gas density too. Therefore, the adopted formula with a temperature-dependence only could be less realistic for describing real ISM evolution influenced by H_2-related physical processes. For example, H_2 cooling is much less efficient in high-density ISM with $n_{\rm H} \sim 10^6$ cm^{-3}, as demonstrated in Figure A1 of Galli & Palla (1998). Although such high-density gaseous regions can be rarely formed owing to the adopted resolution in the present simulations, the model without density-dependent H_2 cooling would mean that (i) the present simulations overestimate the net cooling of gas in disk galaxies and (ii) gas clumps can be more efficiently formed and thus star formation can be more efficient.

The influences of the UV background radiation is not taken into account in the present models either, which means that heating of ISM by the UV background radiation (and internal UV radiation from young massive stars and active galactic nuclei, AGN, in a simulated galaxy) is not properly modeled. This heating of ISM could be more important for the gas dynamical evolution of low-mass disk galaxies where radiative cooling is less efficient owing to lower metallicities. This possible important effect will need to be properly included in our future galaxy-scale simulations with dust-related physical processes.

2.5 Star formation

A gas particle is converted into a 'new star' (collisionless particle) if the following three SF conditions (i)-(iii) are satisfied: (i) the local dynamical time scale is shorter than the sound crossing time scale (mimicking the Jeans instability) , (ii) the local velocity field is identified as being consistent with gravitationally collapsing (i.e., div $\mathbf{v}< 0$), and (iii) the local density exceeds a threshold density for star formation ($\rho_{\rm th}$). This check of gas-to-star-conversion is done at every $0.01 t_{\rm unit}$ (corresponding to the maximum time step width, $\Delta t_{\rm max}$), where $t_{\rm unit}$ is the time units (1.41×10^8 yr) adopted in the present simulations. In our previous simulations, gas-to-star-conversion is done whenever the above three conditions are satisfied. Therefore, the present way to model star formation is a bit different from those in our previous ones.

Star formation can increase dramatically the total number of new stars and dust, if only some fractions of gas particles continue to be converted into new stars at each time step until the mass of the gas particle becomes very small. Since this method is numerically very costly and practically infeasible, we adopt the following SF conversion method. A gas (for which the above three SF conditions are satisfied) is regarded as having a SF probability ($P_{\rm sf}$);

$$P_{\rm sf} = 1 - \exp(-C_{\rm eff} f_{\rm H_2} \Delta t_{\rm max} \rho^{\alpha_{\rm sf}-1}), \quad (7)$$

where $C_{\rm eff}$ corresponds to a star formation efficiency (SFE) in molecular cores and is set to be 0.3. $f_{\rm H_2}$ is the H_2 mass fraction of the gas particle, $\Delta t_{\rm max}$ is the maximum time step width for the particle, ρ is the gas density of the particle, and $\alpha_{\rm sf}$ is the power-law slope of the Kennicutt-Schmidt law (SFR$\propto \rho_{\rm g}^{\alpha_{\rm sf}}$; Kennicutt 1998). A reasonable value of $\alpha_{\rm sf} = 1.5$ is adopted in the present study. This SF probability has been already introduced in our early chemodynamical simulations of galaxies (e.g., Bekki & Shioya 1998). By generating random numbers, we implement this SF method (See B13a and B15 for this).

Each SN is assumed to eject the feedback energy ($E_{\rm sn}$) of 10^{51} erg and 90% and 10% of $E_{\rm sn}$ are used for the increase of thermal energy ('thermal feedback') and random motion

('kinematic feedback'), respectively. The thermal energy is used for the 'adiabatic expansion phase', where each SN can remain adiabatic for a timescale of $t_{\rm adi}$. This adiabatic model is adopted both for SNIa and SNII. Although $t_{\rm adi} = 10^5$ yr is reasonable for a single SN explosion, we adopt a much longer $t_{\rm adi}$ of $\sim 10^6$ yr. This is mainly because multiple SN explosions can occur for a gas particle with a mass of $10^5 {\rm M}_\odot$ in these galaxy-scale simulations, and $t_{\rm adi}$ can be different for multiple SN explosions in a small local region owing to complicated interaction between gaseous ejecta from different SNe. Such interaction of multiple SN explosions would make the adiabatic phase significantly longer in real ISM of galaxies. We adopt a canonical Salpeter stellar initial mass function (IMF) with the slope ($\alpha_{\rm IMF}$) of -2.35 and the upper and lower cutoff masses being $0.1{\rm M}_\odot$ and $100{\rm M}_\odot$, respectively, for all models in the present study.

2.6 Chemical enrichment

The present model for chemical enrichment processes of galaxies is essentially similar to those used in B13a and B15, though the minor details are different between these works. Therefore, we briefly describe only the key elements of the model here. Chemical enrichment through star formation and metal ejection from SNIa, II, and AGB stars is self-consistently included in the chemodynamical simulations. We investigate the time evolution of the 11 chemical elements of H, He, C, N, O, Fe, Mg, Ca, Si, S, and Ba in order to predict both chemical abundances and dust properties in the present study. We consider the time delay between the epoch of star formation and those of supernova explosions and commencement of AGB phases (i.e., non-instantaneous recycling of chemical elements).

We adopt the 'prompt SN Ia' model in which the delay time distribution (DTD) of SNe Ia is consistent with recent observational results by extensive SN Ia surveys (e.g., Mannucci et al. 2006). We adopt the nucleosynthesis yields of SNe II and Ia from Tsujimoto et al. (1995; T95) and AGB stars from van den Hoek & Groenewegen (1997; VG97) in order to estimate chemical yields in the present study. In the present study, ejecta from SNe and AGB stars can become either dust particles or gas-phase metals in gas particles. Therefore, the implementation of chemical enrichment process in the present study with live dust particles is different from those adopted in B13a and B15.

Metals ejected from a stellar particle (SNIa or SNII or AGB star) are assumed to be equally distributed among neighboring SPH gas particles around the stellar particle. These 'neighboring particles' are selected for each SN or AGB star, if SPH particles satisfy the following condition;

$$R \leqslant R_{\rm mix}, \tag{8}$$

where R is the distance between a SPH particle and a SN (or AGB star) and $R_{\rm mix}$ is the 'mixing radius' (parameter). The introduced mixing radius ($R_{\rm mix}$) is set to be the same as the softening length for gas from the stellar particle. Although metals can be locally mixed with gas in this model, the mixing process of metals in real ISM might be more complicated than homogeneous mixing described in the present model. The particle-to-particle abundance differences (corresponding to abundance differences in different local gas clouds) therefore might not be so realistically modeled in the present study.

A new stellar particle ('new star'), which is regarded as a cluster of numerous stars with a given IMF, eject dust and metals only three times: 2.7×10^7 yr (corresponding to SNII explosions, denoted as $t_{\rm SNII}$), 10^8 yr (prompt SNIa explosions, $t_{\rm SNIa}$), and 2.3×10^8 (onset of AGB phases, $t_{\rm AGB}$) after the star formation. A dust particle with chemical elements derived from the adopted IMF and dust yield is created at each ejection process. Therefore, the total mass of a star born at the time $t = t_{\rm form}$ can reduce at each ejection process ($t_{\rm form} < t$). For example, the total mass of j-th element for i-th stellar particle ($m_{{\rm s},i,j}$) after SNII explosions is as follows.

$$m_{{\rm s},i,j}(t = t_{\rm form} + t_{\rm SNII}) = m_{{\rm s},i,j}(t = t_{\rm form}) - m_{{\rm d},i,j} - \Delta m_{{\rm ej},i,j}, \tag{9}$$

where $m_{{\rm d},i,j}$ is the total mass of j-th element of a dust particle produced by i-th stellar particle and $\Delta m_{{\rm ej},i,j}$ is the total mass of j-th element of the ejected gas from i-th stellar particle. The total mass of j-th element of k-th gas particle around i-th stellar particle increases as a result of metal ejection as follows:

$$m_{{\rm g},k,j}(t = t_{\rm form} + t_{\rm SNII}) = m_{{\rm g},k,j}(t = t_{\rm form}) + \Delta m_{{\rm ej},i,j}/N_{{\rm nei},i}, \tag{10}$$

where $N_{{\rm nei},i}$ is the total number of gas particles around the stellar particle (i.e., within the SPH-smoothing length, h_k, for k-th gas particle). By replacing $t_{\rm SNII}$ with $t_{\rm SNIa}$ and $t_{\rm AGB}$, we can estimate the mass evolution of stellar and gaseous particles due to SNIa explosions and stellar mass loss of AGB stars.

We limit the number of dust and metal ejection to only three times, because we need to avoid an unnecessarily large number of particles that can virtually make it impossible for us to simulate galaxy evolution owing to the dust-related calculations. The dust particles initially in thin disks and those from SNIa, SNII, and AGB stars are labeled as 'old', 'SNIa', 'SNII', and 'AGB' dust, respectively. The maximum total number of particles of a simulation for which we can finish all calculations of a model within a reasonable timescale (less than a week) on a single GPU server (Tesla K10 used in this paper) is around 2×10^6. This means that we need to have a massively parallel cluster to run $N \sim 10^8 - 10^9$ for cosmological hydrodynamical simulations with dust dynamics and recycling. We discuss how to implement the present new code to run on such a large cluster in our forthcoming papers.

The initial chemical abundances and dust properties are different in different gas particles and given according to the positions of the particles within its host disk galaxy. The gas-phase metallicity of each (gaseous and stellar) particle is given according to its initial position: at $r = R$, where r (R) is the projected distance (in units of kpc) from the center of the disk, the metallicity of the star is given as:

$$[{\rm Fe/H}]_{\rm r=R} = [{\rm Fe/H}]_{\rm d,r=0} + \alpha \times {\rm R}. \tag{11}$$

where α is the slope of the metallicity gradient in units of dex kpc^{-1}. We show the results of the models with $\alpha = -0.04$, which is the observed value of our Milky Way (e.g., Andrievsky et al. 2004).Initial dust-to-metal-ratio is set to

Table 3. Description of the basic parameter values for the three different disk galaxy models.

Model name/Physical properties	MW-type	LMC-type	Dwarf-type	Sa-type
DM mass ($\times 10^{12} M_\odot$)	1.0	0.1	0.01	1.0
Virial radius (kpc)	245.0	113.8	52.9	245.0
c [a]	10	12	16	10
Stellar disk mass ($\times 10^{10} M_\odot$)	6.0	0.36	0.036	6.0
Gas disk mass ($\times 10^{10} M_\odot$)	0.6	0.18	0.0036	0.6
Bulge mass ($\times 10^{10} M_\odot$)	1.0	–	–	12.0
Dust-to-gas-ratio [b]	0.0064	0.0064	0.0064	0.0064
Dust-to-metal-ratio	0.4	0.4	0.4	0.4
Initial central gas-phase metallicity ($[Fe/H]_0$)	0.34	−0.28	−1.04	0.34
Radial metallicity gradient (dex kpc^{-1})	−0.04	−0.04	−0.04	−0.04
Stellar disk size (kpc)	17.5	8.1	3.8	17.5
Gas disk size (kpc)	35.0	16.2	7.6	35.0
Bulge size (kpc)	3.5	–	–	17.2
Gas disk size (kpc)	35.0	16.2	7.6	35.0
DM particle mass ($\times 10^6 M_\odot$)	1.4	0.14	0.014	1.4
Gas particle mass ($\times 10^4 M_\odot$)	6.0	1.8	0.36	6.0
DM softening length ($\epsilon_{\rm DM}$)	2.1 kpc	0.6 kpc	0.17 kpc	2.1 kpc
Gas softening length ($\epsilon_{\rm g}$)	0.2 kpc	0.063 kpc	0.02 kpc	0.2 kpc

[a] c is the c-parameter in the NFW dark matter profiles.
[b] The value is adopted from observational results by Zubko et al. 2004.

be 0.4 for all particles in a simulation. The central metallicity $[Fe/H]_{d,r=0}$ is simple referred to as $[Fe/H]_0$ and it is different in different galaxy models with different masses.

2.7 Dust growth and destruction

Although the dust model adopted in the present study is similar to those adopted by B13a and B15, there are some differences between these models owing to the newly adopted live dust particle method. We here describe the model with special emphasis on the model differences. We calculate the total mass of jth component (j=C, O, Mg, Si, S, Ca, and Fe) of dust from kth type of stars (k = I, II, and AGB for SNe Ia, SNe II, and AGB stars, respectively) based on the methods described in B13a that is similar to those adopted in D98. We consider that the key parameter in dust accretion is the dust accretion timescale ($\tau_{\rm a}$). In the present study, this parameter can vary between different gas particles and is thus represented by $\tau_{{\rm a},l}$ for lth gas particle.

The mass of jth component (j=C, O, Mg, Si, S, Ca, and Fe) of ith dust particle at time t can increase owing to metal accretion onto the dust from the surrounding gas particles. The mass increase of jth element of ith dust particle due to the metal-transfer between gas and dust particles is described as

$$\Delta m^{\rm acc}_{{\rm d},i,j}(t) = \Delta t_i m_{{\rm g,mean},i,j}(t)/\tau_{{\rm a,mean},i}, \quad (12)$$

where Δt_i is the individual time step width for ith dust particle and $m_{{\rm g,mean},i,j}$ is the mean mass of jth chemical element for all gas particles around ith dust particle, and $\tau_{{\rm a,mean},i}$ is the mean dust accretion timescale for the gas particles. In order to estimate $m_{{\rm g,mean},i,j}$ and $\tau_{{\rm a,mean},i}$, we choose a gas particle as a surrounding particle around ith dust particle if it satisfies the following condition:

$$R \leqslant R_{\rm grow}, \quad (13)$$

where R is the distance between the gas particle and ith dust particle and $R_{\rm grow}$ is a parameter for this neighbor particle search. Since dust particles do not have smoothing length like SPH particles, we have to introduce this parameter $R_{\rm grow}$. This $R_{\rm grow}$ is set to be $0.5\epsilon_{\rm g}$ (where $\epsilon_{\rm g}$ is the gravitational length for gas), and the dependence of the present results on $R_{\rm grow}$ is discussed in Appendix B.

Therefore, $m_{{\rm g,mean},i,j}$ and $\tau_{{\rm a,mean},i}$ are estimated as follows:

$$m_{{\rm g,mean},i,j} = \frac{1}{N_{{\rm nei},i}} \sum_{k=1}^{N_{{\rm nei},i}} m_{{\rm g},k,j}, \quad (14)$$

and

$$\tau_{{\rm a,mean},i} = \frac{1}{N_{{\rm nei},i}} \sum_{k=1}^{N_{{\rm nei},i}} \tau_{{\rm a},k}, \quad (15)$$

where $\tau_{{\rm a},k}$ is the dust growth timescale for kth gas particle. These ways to estimate dust growth become different from our previous ones (the equation 9) in B13a because of the adopted live dust particle method. Owing to this dust growth, the mass of jth chemical component of kth gas particle is reduce and this reduction is estimated at each time step.

Dust grains can be destroyed though supernova blast waves in the ISM of galaxies (e.g., McKee 1989) and the destruction process is parameterized by the destruction time scale ($\tau_{\rm d}$) in previous one-zone models (e.g., Lisenfeld & Ferrara 1998; Hirashita 1999). Although B13a and B15 adopted a model similar to these one-zone models, the present study adopts a different one. The decrease of the mass of jth component of ith dust particle at time t due to dust destruction process is as follows

$$\Delta m^{\rm dest}_{{\rm d},i,j}(t) = -f_{{\rm dest},i} m_{{\rm d},i,j}(t) \quad (16)$$

where $f_{\rm dest,}$ is the mass fraction of dust destroyed by SNe and assumed to be a free parameter in the present study. The possibly reasonable range of this parameter will be dis-

cussed later in this paper. Although $f_{\rm dust}$ can be different depending on the physical conditions of ISM (e.g., Jones et al. 1995), we adopted a simplified assumption of a fixed $f_{\rm dest}$ in this study. The dust destroyed by SNe can be returned back to the ISM, and therefore $f_{{\rm dest},i} m_{{\rm d},i,j}(t)/N_{{\rm nei},i}$ is added to each of the neighboring gas particle around the dust particle. This mass increase and decrease is estimated only when SNII and SNIa explosions occur for each stellar particle. This metal-transfer calculation is done for gas particles, if the particles satisfy the following condition;

$$R \leqslant R_{\rm dest}, \tag{17}$$

where R is the distance between a SPH particle and a SN and $R_{\rm dest}$ is the 'destruction radius'. This destruction radius is set to be the same as the mixing radius ($R_{\rm mix}$) for SNe.

Thus the equation for the time evolution of jth component of metals for ith dust particle is given as

$$m_{{\rm d},i,j}(t + \Delta t_i) = m_{{\rm d},i,j}(t) + \Delta m^{\rm acc}_{{\rm d},i,j}(t) + \Delta m^{\rm dest}_{{\rm d},i,j}(t) \tag{18}$$

When star formation occurs in a molecular cloud, dust can be consumed by star formation and locked up in planets around stars. In the present study, we do not consider this dust consumption by star and planet formation, mainly because we need to introduce another sets of model parameters. The total mass of dust locked up in stars and planets could be significantly smaller than the total amount of dust grown from ISM and produced by stars. We discuss this important issue in our forthcoming papers.

The dust accretion time scale, τ_a, is assumed to be different between different particles with different gaseous properties and changes with time according to the changes of gaseous properties in the present study. In adopting this variable dust accretion ('VDA') model, we introduce a few additional parameters in VDA in order to describe the possible dependences of $\tau_{\rm a}$ of gas particles on the gas densities, temperature, and chemical abundances. Our previous simulations with VDA (B15) have already demonstrated the importance of dust accretion and destruction in the evolution of dust-to-gas-ratios (D) and H_2 mass fractions ($f_{\rm H_2}$). Since the details of the VDA model is given in (B15), we describe only the key ingredients of the VDA model below.

We adopt the following dependence of $\tau_{{\rm a},i}$ on the mass density and temperature of ith gas particle in the VDA:

$$\tau_{{\rm a},i} = \tau_0 (\frac{\rho_{\rm g,0}}{\rho_{{\rm g},i}}) (\frac{T_{\rm g,0}}{T_{{\rm g},i}})^{0.5}, \tag{19}$$

where $\rho_{{\rm g},i}$ and $T_{{\rm g},i}$ are the gas density and temperature of i-th gas particle, respectively, $\rho_{\rm a,0}$ (typical ISM density at the solar neighborhood) and $T_{\rm g,0}$ (temperature of cold gas) are set to be 1 atom cm^{-3} and 20K, respectively, and τ_0 is a reference dust accretion timescale at $\rho_{\rm g,0}$ and $T_{\rm g,0}$. As discussed in B15, galaxy-scale simulations like the present ones can not resolve the atomic-scale physics of dust growth (much smaller than the possible resolution of the present simulations). Therefore, the above $\tau_{{\rm a},i}$ for a gas particle should be regarded as the dust growth timescale averaged over the smoothing length of the particle ($10 - 100$ pc). As shown in previous one-zone models (e.g., D98) and our previous simulations (B13a), the dust accretion time-scale should be an order of 10^8 yr so that the observed dust abundances and $f_{\rm H_2}$ can be reproduced. We therefore adopt $\tau_{\rm a,0} = 2 \times 10^8$ yr for all models of the present study.

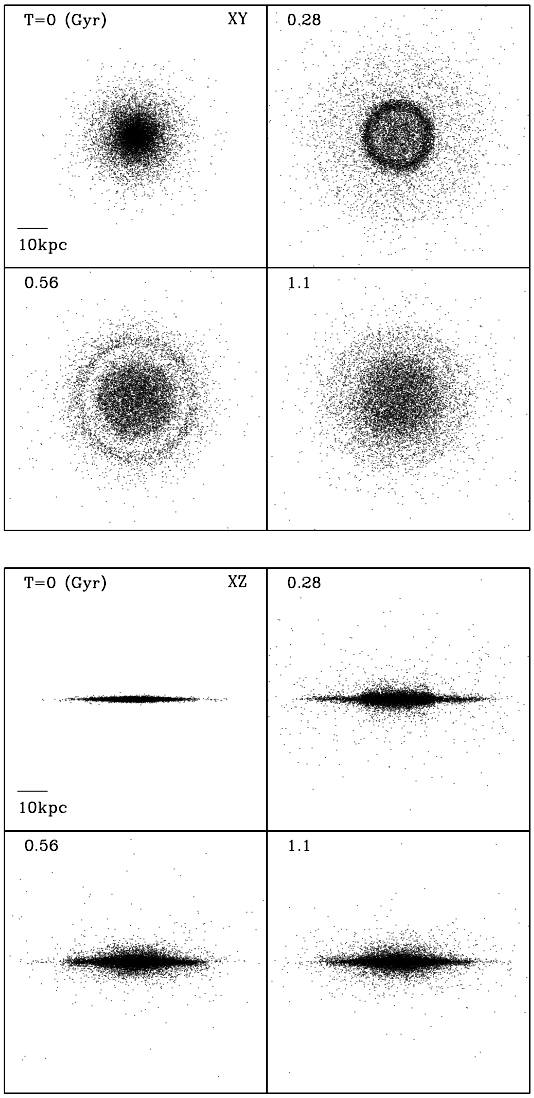

Figure 1. The time evolution of the mass distribution of silicate projected onto the x-y plane (upper four) and onto the x-z plane (lower four) for the fiducial MW-type disk model with stellar radiation pressure. Only one every ten particles is plotted to reduce the file size of this figure (yet the detail of the dust distribution can be clearly seen). The time T in the upper left corner of each panel indicates time that has elapsed since the simulation started.

2.8 H_2 formation and dissociation

The H_2 formation and dissociation processes can be regulated by dust evolution, because the major formation sites of H_2 is on dust grains. The model for these processes adopted in the present study is exactly the same as those used in B13a: H_2 formation on dust grains and H_2 dissociation by FUV radiation are both self-consistently included in chemodynamical simulations. Recent theoretical studies on H_2 formation on dust grains have revealed the important roles of dust temperature and its random fluctuation in H_2 formation on dust grains (e.g. Bron et al. 2014). We however do not include these, mainly because dust temperature and its fluctuation for each dust particle can not be reliably derived

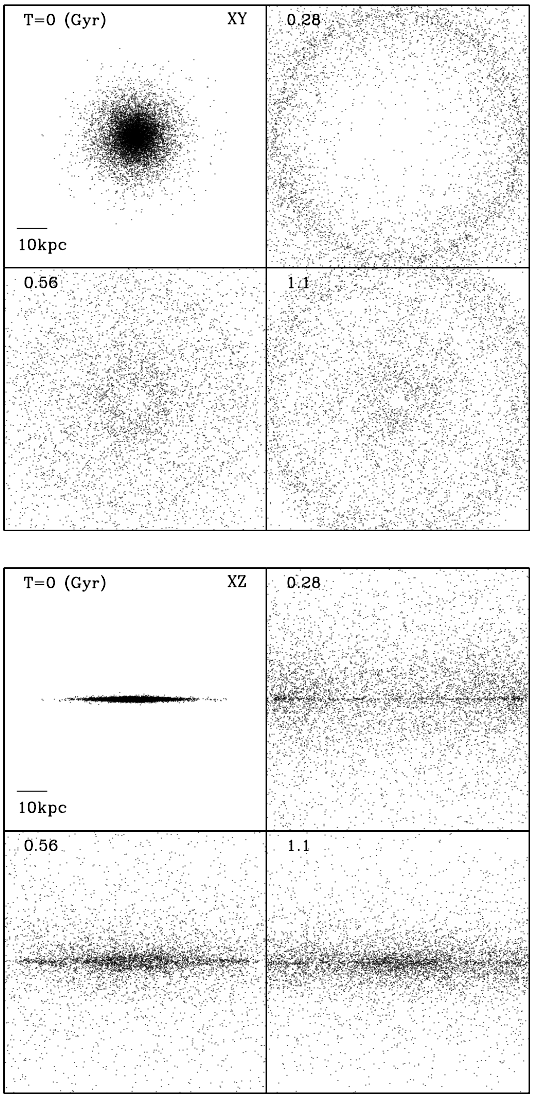

Figure 2. The same as Fig. 1 but for the distribution of graphite. The more extended distribution of graphite in this figure is due to the combination of the adopted small dust size and $A_{\rm t} = 0$ mag. The models with larger $A_{\rm t}$ show less extended distributions of dust.

in the present simulation without a realistic model for dust temperature estimation.

The temperature ($T_{\rm g}$), hydrogen density ($\rho_{\rm H}$), dust-to-gas ratio (D) of a gas particle and the strength of the FUV radiation field (χ) around the gas particle are calculated at each time step so that the fraction of molecular hydrogen ($f_{\rm H_2}$) for the gas particle can be derived based on the H_2 formation/destruction equilibrium conditions. Thus the H_2 fraction for i-th gas particle ($f_{{\rm H}_2,i}$) is given as;

$$f_{{\rm H}_2,i} = F(T_{{\rm g},i}, \rho_{{\rm H},i}, D_i, \chi_i), \quad (20)$$

where F means a function for $f_{{\rm H}_2,i}$ determination. The standard value (3×10^{-17} cm^3 s^{-1}) for the total volume H_2 formation rate is adopted for all models of the present study.

Since the detail of the derivation methods of χ_i and $f_{{\rm H}_2,i}$ (thus F) are given in B13a and B15, we here briefly describe the methods. The SEDs of stellar particles around each i-th gas particles (thus ISRF) are first estimated from ages and metallicities of the stars by using stellar population synthesis codes for a given IMF (e.g., Bruzual & Charlot 2003). Then the strength of the FUV-part of the ISRF is estimated from the SEDs so that χ_i can be derived for the i-th gas particle. Based on χ_i, D_i, and $\rho_{{\rm H},i}$ of the gas particle, we can derive $f_{{\rm H}_2,i}$ (See Fig. 1 in B13a). Thus each gas particle has $f_{{\rm H}_2,i}$, metallicity ([Fe/H]), and gas density, all of which are used for estimating the IMF slopes for the particle (when it is converted into a new star). The ages of stars (t_0) are assumed to be free parameters ranging from 0.1 Gyr and 10 Gyr in the present study.

Table 4. Description of the fiducial model.

Disk model	MW-type
Dust type	silicate (S) or graphite (G)
RP	Yes
PEH	No
GD	No
CR	No
DR	No
Dust growth	Yes
Dust destruction	No
$R_{\rm grow}$	$0.5\epsilon_{\rm g}$
$A_{\rm t}$	0 mag
t_0	5 Gyr
$N_{\rm dust}$	10^5
$\rho_{\rm dust,S}$	3.0 g cm^{-3}
$R_{\rm dust,S}$	0.1 μm
$\rho_{\rm dust,G}$	2.3 g cm^{-3}
$R_{\rm dust,G}$	0.05 μm
IMF	Salpeter ($\alpha_{\rm IMF} = -2.35$)
SSP	Bruzual & Charlot (2003)

Table 5. The adopted values of four key parameters.

Parameter	Adopted values
Dust type	silicate, graphite
$A_{\rm t}$	0, 0.3, 1, 2 (mag)
t_0	1, 3, 5, 10 (Gyr)
$Q^*_{\rm rp}$	0, 0.5, 1, 2

2.9 Photo-electric heating by dust

Heating of ISM through the photo-electric ('PEH') ejections of electrons from dust grains interacting with ISRF has been discussed by many theoretical works (e.g., Watson 1972; Draine 1978; Bakes & Tielens 1994, BT94). These works clearly demonstrated that the photo-electric heating is important in the thermal history of ISM and the level of this importance depends on the detailed physical conditions of ISM, such as the strength of ISRF and dust size distributions (e.g., BT94). We here include this important photo-electric heating in our galaxy-scale simulations in such a way that the net heating rate is estimated for each gas particle according to the physical properties of the gas particle and those of dust particles around the gas particle. Since our estimation of the photo-electric heating rate is estimated directly from gas and dust properties, our model is much better than those adopted in other galaxy-scale simulations with photo-electric heating (e.g., Tasker 2011) in which the evolution of ISRF and dust abundances is not considered.

We adopt the analytic formula for photo-electric heating rate ($n\Gamma_{\rm pe}$) proposed by BT94 as follows:

$$n\Gamma_{\rm pe} = 1.0 \times 10^{-24} \epsilon n G_0 \ {\rm ergs \ cm^{-3} \ s^{-1}}, \quad (21)$$

where n is the number density of gas, ϵ is the heating efficiency, and G_0 is the intensity of the incident far-UV field in units of Habing interstellar radiation field. BT94 showed that (i) ϵ depends mainly on G_0, $T_{\rm g}$, and $n_{\rm e}$, where $n_{\rm e}$ is the electron number density, in ISM (e.g., equation 43 in BT94) and (ii) ϵ ranges from 0.001 to 0.05 within their models. Although our simulations can output G_0, n, and $T_{\rm g}$, $n_{\rm e}$ is not the direct output of our simulations. We therefore assume that ϵ is a parameter for a model in the present study. We mainly show the results of the models with $\epsilon = 0.003$ in the present study, and our forthcoming papers will discuss how ϵ can control thermal evolution of ISM in galaxies.

In estimating G_0 for each gas particle, we need to consider that not all of the FUV flux of a star around the gas particle can be used for photo-electric heating owing to dust extinction. The flux at a wavelength λ for ith star around jth gas particle in a screen model can be given as follows

$$f_{\lambda,i} = f_{\lambda,0,i} e^{-\tau_{\lambda,j} r_{i,j}/h_j}, \quad (22)$$

where $f_{\lambda,0,i}$ is the original flux of the star, $\tau_{\lambda,j}$ is the optical depth (i.e. $\tau_\lambda \approx 0.921 A_\lambda$), $r_{i,j}$ is the distance of the gas and the star, and h_j is the SPH smoothing length of the gas particle. Therefore, the G_0 factor for photo-electric heating of jth gas particle from ith stellar particle ($G_{0,i,j}$) is

$$G_{0,i,j} = F_{{\rm ext},i,j} g_{0,i,j}, \quad (23)$$

where $g_{0,i,j}$ is G_0 estimated by assuming no dust extinction and $F_{{\rm ext},i,j}$ is the fraction of light absorbed by dust and given as follows:

$$F_{{\rm ext},i,j} = \int_0^1 e^{-\tau_j r} dr, \quad (24)$$

where τ_j is the FUV optical depth and a fixed value is used. Since the adopted SPH kernel is 0 at h_j, the above integration range needs to be from 0 to 1. In deriving τ_j, we first estimate the optical dust extinction ($A_{{\rm V},j}$) based on the gas column density ($N_{{\rm H},j}$) and the dust-to-gas-ratio (D_j). Then we estimate $A_{{\rm FUV},j}$ from $A_{{\rm V},j}$ by using the Calzett's extinction law (i.e., the equation (4) in Calzetti et al. 2000). In estimating $A_{{\rm V},j}$, we use the following observational results around the solar neighborhood (Predehl & Schmitt 1995):

$$\frac{N_{\rm H}}{A_{\rm V}} = 1.8 \times 10^{21} \ {\rm atoms \ cm^{-2} \ mag^{-1}}. \quad (25)$$

Accordingly, $A_{{\rm V},j}$ is linearly proportional to $N_{{\rm H},j}$ and D_j. The ratio of $A_{\rm FUV}$ to $A_{\rm V}$ is estimated to be 2.56 and this fixed value is used for all gas particles to derive $A_{\rm FUV}$ (thus $\tau_{\rm FUV}$). The local column density $N_{{\rm H},j}$ is estimated as $\rho_j({\rm H}) h_j$, where $\rho_j({\rm H})$ is the 3D hydrogen density and h_j is the smoothing length for the SPH gas particle. Thus G_0 can be estimated from physical properties of gas and dust in a self-consistent manner.

2.10 Cosmic-ray heating

Although gas heading by cosmic-ray ('CR') would not be so efficient as photo-electric heating in typical ISM of star-forming galaxies ($n \sim 1$ atom cm^{-3}, SFR$\sim$ 1 M$_\odot$ yr^{-1}), it can be important in thermal histories in some galaxy environments (e.g., central starburst regions). We therefore include this cosmic-ray heating by using the following analytic formula described in Tielens (2005);

$$n\Gamma_{\rm CR} = 3.0 \times 10^{-27} n (\frac{\zeta_{\rm CR}}{2 \times 10^{-16}}) \ {\rm ergs \ cm^{-3} \ s^{-1}}, \quad (26)$$

where $\zeta_{\rm CR}$ is total cosmic ionization rate. If cosmic ray originates from SNe, then it is reasonable for us to assume that the total flux of comic ray in a galaxy is proportional to the SFR of the galaxy. We therefore assume that $\zeta_{\rm CR}$ is $2 \times 10^{-16} (\frac{\rm SFR}{1.3 {\rm M}_\odot {\rm yr}^{-1}})$ s^{-1}, where the reference SFR of 1.3M$_\odot$ yr^{-1} corresponds to the present SFR of the Galaxy (e.g., Draine 2009). We admit that there is a great uncertainty in the scaling relation between $\zeta_{\rm CR}$ and SFRs of galaxies. Accordingly, it would be better for the present study to discuss the roles of dust in the evolution of ISM by *not* including cosmic-ray heating.

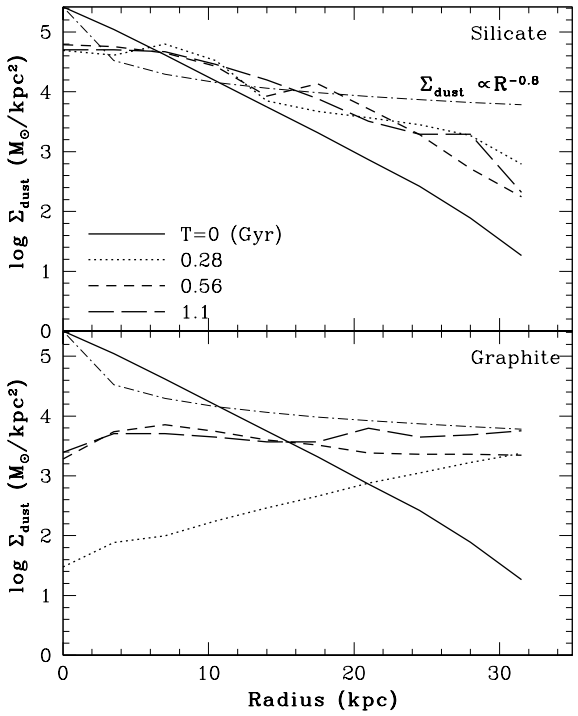

Figure 3. The projected radial mass density profiles of silicate (upper) and graphite (lower) at four selected time steps in the fiducial MW-type disk model. The radius (R) in this figure is the distance from the center of galaxy in the x-y plane ($R = \sqrt{x^2+y^2}$). The solid, dotted, short-dashed, and long-dashed lines indicate the dust distributions at $T = 0$, 0.26, 0.56, and 1.1 Gyr, respectively. For comparison, the observed rather flat distribution of dust around galaxies (M10) is shown by a dot-dashed line with an arbitrary $\Sigma_{\rm dust}$ at $R = 0$.

2.11 Gas-dust heating

In principle, we can estimate separately the temperature of gas ($T_{\rm g}$) and that of dust ($T_{\rm d}$) in the present study with the new live dust particle method. If $T_{\rm d}$ is higher than $T_{\rm g}$, then ISM can be heated up. Given that the observed mean $T_{\rm d}$ is around $20-30$K (Dunne et al. 2001) and thus not so

different, this dust-gas heating would be important only for a small amount of gas in galaxies. We adopt the following formula (Tielens 2005) for the estimation of dust-gas cooling rate:

$$n\Gamma_{\rm gd} = 1.0 \times 10^{-33} n T_{\rm g}^{0.5} (T_{\rm d} - T_{\rm g}) \ {\rm ergs \ cm^{-3} \ s^{-1}}. \quad (27)$$

In order to derive $T_{\rm d}$, we use the observed scaling relation between $T_{\rm d}$ and $L_{\rm FIR}$ (total FIR luminosity) by Amblard et al. (2010) as follows:

$$T_{\rm d} \ ({\rm K}) = -20.5 + 4.4 \log(L_{\rm FIR}/L_\odot). \quad (28)$$

We estimate $L_{\rm FIR}$ from the observed relation between SFR and $L_{\rm FIR}$ (Kennicutt 1998) as follows:

$$\frac{\rm SFR}{\rm M_\odot yr^{-1}} = \frac{L_{\rm FIR}}{5.8 \times 10^9 {\rm L_\odot}}. \quad (29)$$

In the above estimation of $\Gamma_{\rm gd}$, the dust temperature of a galaxy is estimated by using the galactic SFR and $T_{\rm d}$ is used for all gaseous particles. This method is clearly over-simplified, though such a simple model could possibly grasp some essential ingredients of dust-gas heating in ISM evolution. We therefore do not include the adopted dust-gas heating in most of the present simulations. We just briefly discuss how the possible effects of dust-gas heating on ISM are for a number of models. As Bekki & Shioya (2000) has already shown, $T_{\rm d}$ can be estimated for each particle by using radiation-transfer models for arbitrary geometry of a galaxy modeled by Nbody + gas dynamical simulations. In our forthcoming papers, we need to estimate $T_{\rm d}$ for each dust particle so that we can discuss the roles of dust-gas heating in ISM evolution in a more convincing manner.

2.12 Gaseous drag effects on dust

Theis & Orlova (2004) first investigated the roles of dust in dynamical evolution of ISM in the central regions of galaxies and thereby found that the central gas disks can become dynamically unstable if the mass fractions of dust in the disks exceed 2%. These results imply that gas-dust coupling by a drag force in ISM can be an important aspect of ISM evolution in galaxies. However, the frictional (drag) timescale ($\tau_{\rm drag}$, which corresponds to the timescale for momentum transfer between gas and dust through gas-dust collision) is rather short (an order of $10^3 - 10^4$ yr) for ISM with typical dust sizes and masses. The maximum time-step width, $\Delta t_{\rm max}$ ($\sim 10^6$ yr), in the present simulations is significantly longer than $\tau_{\rm drag}$. Therefore, it would be reasonable for us to assume that even if gas and dust initially have different velocities, they come to have identical velocities within $\Delta t_{\rm max}$.

However, $\tau_{\rm drag}$ can be longer than $\Delta t_{\rm max}$ in some local regions during the evolution of ISM. We accordingly investigate how the gaseous drag can influence the evolution of dust in galaxies by adopting the model below. The frictional drag force ($F_{\rm drag}$) between gas and dust is described as follows:

$$\mathbf{F}_{\rm drag} = -C_{\rm drag} \eta_{\rm dust} (\mathbf{v}_{\rm d} - \mathbf{v}_{\rm g}), \quad (30)$$

where $\mathbf{v}_{\rm d}$ and $\mathbf{v}_{\rm g}$ are the velocity vectors of dust and gas, respectively, and $\eta_{\rm dust}$ is $m_{\rm d}/m_{\rm dust}$ (where $m_{\rm d}$ is the dust particle mass and $m_{\rm dust}$ is the mass of a dust grain): this $\eta_{\rm dust}$ needs to be considered, because this $F_{\rm drag}$ is for a dust partilce (not for a dust grain). The coefficient $C_{\rm drag}$ corresponding to $\tau_{\rm drag}^{-1}$ (Noh et al. 1991; Theis & Orlova 2004) is given as

$$C_{\rm drag} = \frac{\sigma_{\rm c} \rho_{\rm g} v_{\rm th}}{m_{\rm dust}}, \quad (31)$$

where $\sigma_{\rm c}$, $\rho_{\rm g}$, $v_{\rm th}$, and $m_{\rm dust}$ are the cross section of a dust grain ($\sigma_{\rm c} = \pi R_{\rm dust}^2$, where $R_{\rm dust}$ is the dust size), the mass density of the gas, the thermal velocity of the gas, and the total mass of the grain. It should be stressed here that this $m_{\rm dust}$ is not the mass of a dust particle in a simulation.

In implementing the above drag effects for each dust particle in a simulation, we need to consider that $F_{\rm drag}$ for ith dust particle ($F_{{\rm drag},i}$) is the force from all gas particles around the dust particle, as follows:

$$\mathbf{F}_{{\rm drag},i} = \mathbf{f}_{{\rm drag},i,j}, \quad (32)$$

where $\mathbf{f}_{{\rm drag},i,j}$ is the drag force between ith dust particle and jth gas particle that is the nearest to the dust particle. This $f_{{\rm drag},i,j}$ is calculated from the velocities of the particles and $C_{\rm drag}$. The back-reaction of the drag force needs to be considered for jth gas particle because of momentum conservation as follows:

$$\mathbf{F}_{{\rm drag},j} = -m_{{\rm d},i} \mathbf{f}_{{\rm drag},i,j} / m_{{\rm g},j}. \quad (33)$$

These drag terms are added to the equations of motion at each time step.

2.13 Radiation pressure of stars on dust

Barsella et al. (1989) and F91 investigated how radiation pressure of stars on dust grains can influence their orbital evolution around their host galaxy by using some idealized models in which both the gravitational potential and the light distribution of the galaxy are fixed during dust evolution. Here we improve their model by calculating the light and mass distributions of a galaxy at every time step so that we can better estimate the 3D radiation field of the galaxy. For each ith dust particle, $F_{{\rm rad},i}$ is the sum of the force due to radiation pressure from all stars as follows (e.g., Barsella et al. 1989):

$$\mathbf{F}_{{\rm rad},i} = \frac{\pi \eta_{\rm dust} R_{\rm dust}^2 Q_{\rm pr}^*}{c} \sum_{j=1}^{N_{\rm s}} L_{{\rm s},j} \frac{\mathbf{x}_i - \mathbf{x}_j}{4\pi |\mathbf{x}_i - \mathbf{x}_j|^3}, \quad (34)$$

where $Q_{\rm pr}^*$ is the frequency-averaged radiation pressure coefficient for a grain, c is the speed of light, $N_{\rm s}$ is the total number of stellar particles, $L_{\rm j}$ is the total luminosity of jth stellar particle, $\mathbf{x}_i$ is the 3D position vector of ith dust particle, and $\mathbf{x}_j$ is the 3D position vector of jth stellar particle. Since this is $F_{\rm rad}$ for a dust particle, the $\eta_{\rm dust}$ factor needs to be considered.

In order to estimate $L_{{\rm s},j}$ for jth stellar particle with a metallicity and an age, we use the stellar population synthesis code by Bruzual & Charlot 2003) for the adopted IMF. By considering dust extinction, we can estimate $L_{{\rm s},j}$ as follows:

$$L_{{\rm s},j} = m_{{\rm s},j} \Upsilon_j^{-1} e^{-0.921 A_j}, \quad (35)$$

where Υ_j is the mass-to-light-ratio derived from the stellar population synthesis code for jth stellar particle and A_j is the dust extinction for the particle. If we estimate A_j in

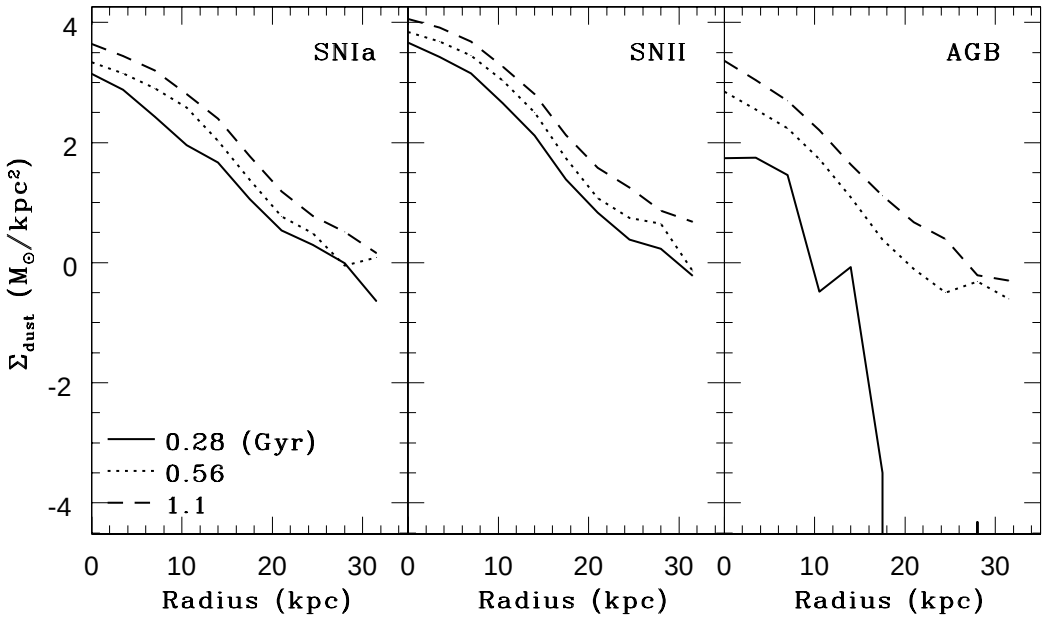

Figure 4. The projected radial mass density profiles of newly produced dust from SNIa (left), SNII (middle), and AGB stars (right) in the fiducial MW-type disk model. The solid, dotted, and short-dashed lines indicate the dust profiles at T=0.28, 0.56, and 1.1 Gyr, respectively.

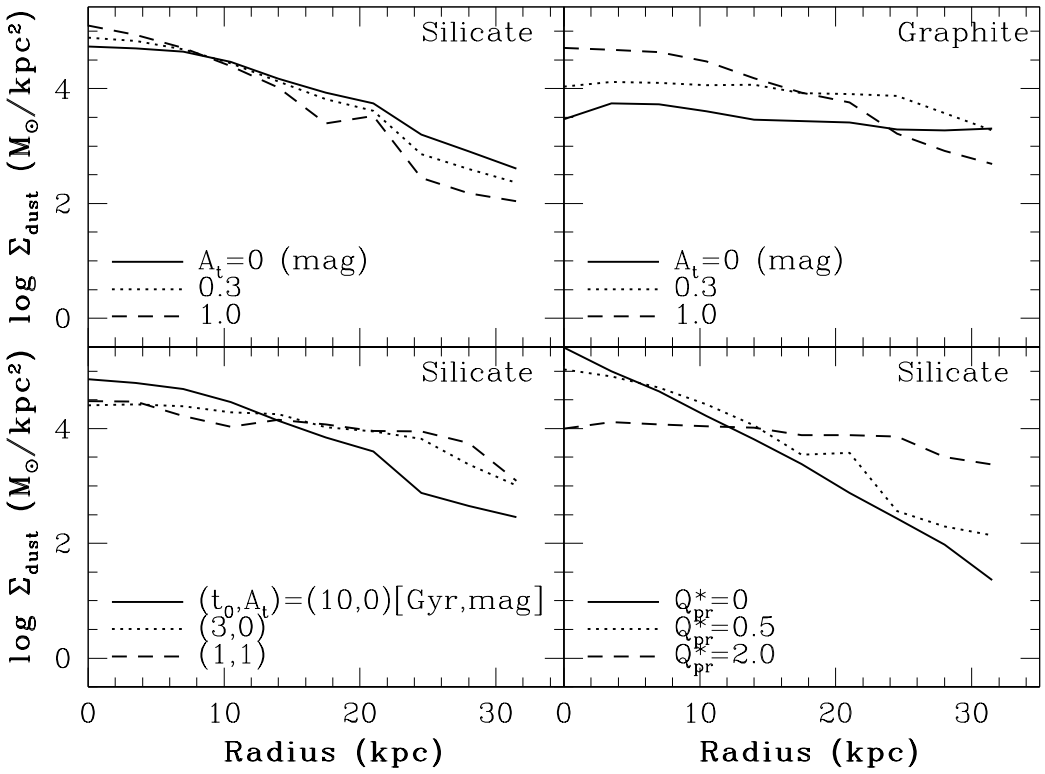

Figure 5. The final projected radial mass profiles of dust in different 12 MW-type disk models with stellar radiation pressure. The upper left and right panels shows the profiles of silicate and graphite, respectively, for $A_{\rm t}$ = 0, (solid), 0.3 (dotted), and 1.0 mag (short-dashed). The lower left panel shows the profiles of silicate in the models with ($t_0, A_{\rm t}$=(10,0) (solid) =(3,0) (dotted) (1,1) [Gyr, mag] (solid) (solid), 0.3 (dotted), and 1.0 mag (short-dashed). The solid, dotted, and short-dashed lines in the lower right panel indicate $Q^*_{\rm pr}$ = 0, 0.5, and 2.0, respectively. The model with $Q^*_{\rm pr}$ = 0 corresponding to 'no radiation pressure'.

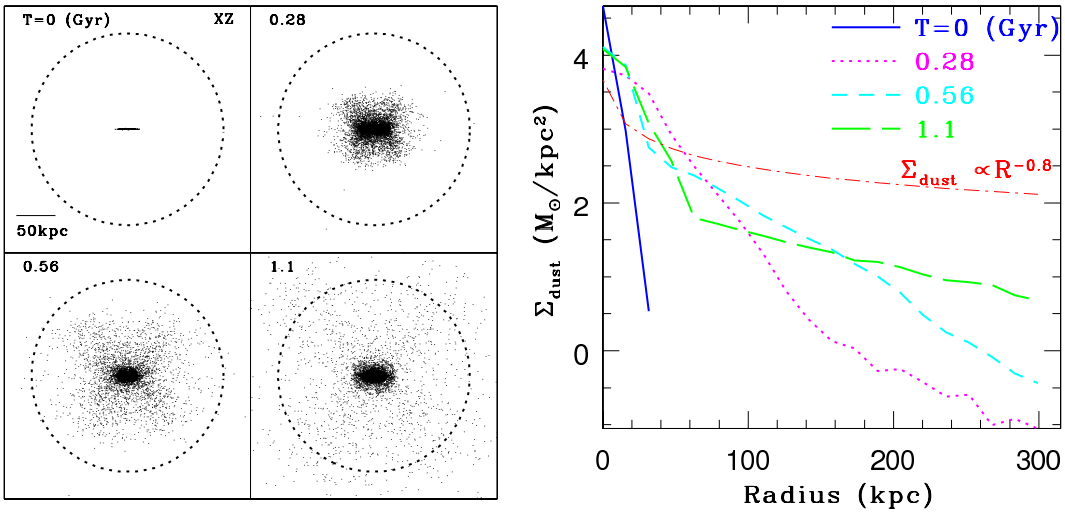

Figure 6. The time evolution of graphite distributions projected onto the x-z plane in the MW-type disk model with radiation pressure and $A_{\rm t} = 0.3$ mag (left) and the projected radial density profiles of graphite for the selected four time steps (right). The virial radius of the dark matter halo is shown by a thick dotted line in the left panel. The blue solid, magenta dotted, cyan short-dashed, and green long-dashed lines indicate $T = 0$, 0.28, 0.56, and 1.1 Gyr, respectively in the right panel. For comparison, the observed profile of dust around galaxies by M10 is shown by a red dot-dashed line with an arbitrary $\Sigma_{\rm dust}$ at $R = 0$.

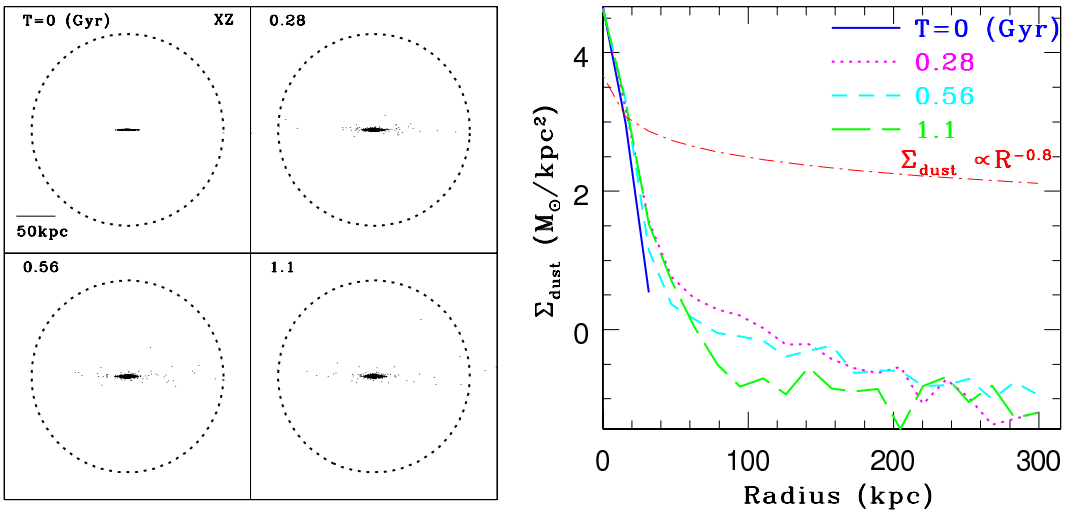

Figure 7. The same as Fig. 6 but for the silicate distribution in the MW-type disk with radiation pressure and heavy dust extinction ($A_{\rm t} = 1$ mag). It should be stressed here that dust can not be so extended in the vertical direction owing to the much weaker stellar radiation field in this model.

a fully self-consistent manner, we need to do so by investigating the column densities and dust abundances of all gas particles that the light of jth stellar particle can pass through while it is traveling to ith dust particle. This means that the required time for the calculation of $F_{\rm rad}$ for just one dust particle is proportional to $N_{\rm s}N_{\rm g}$: thus the calculations for all dust particles at each time step is proportional to $N_{\rm d}N_{\rm s}N_{\rm g}$ (virtually $\propto N^3$). This calculation is very numerically costly and thus infeasible unless a fast method for this calculation is developed. We therefore investigate the models with a fixed (total) dust extinction ($A_{\rm t}$) in which $A_{\rm t}$ is 0, 0.3, 1. and 2 mag. By comparing the model with different $A_{\rm t}$, we can better understand how dust extinction can be important for the evolution of dust being influenced by radiation pressure of stars in galaxies.

Following F91, we investigate mainly two dust species: interstellar silicate with $R_{\rm dust} \sim 0.1$ μm and $\rho_{\rm dust} = 3.0$ g cm^{-3} and graphite with $R_{\rm dust} \sim 0.05$ μm and $\rho_{\rm dust} = 2.3$ g cm^{-3}. In order to demonstrate the roles of radiation pressure of stars in the evolution of dust more clearly, interstellar dust is assumed to be either of the above silicate or graphite in the present simulations. Given that interstellar dust consists of different grains with different compositions and sizes, this is obviously an over-simplification. Although we admit this, we think that we need to start this investigation with a somewhat idealized model in order to grasp some essential ingredients of stellar radiation pressure on dust dynamics. We therefore try to understand the influences of stellar radiation pressure on dust evolution by using a simpler model in the present study, and will construct a more realistic and

complicated model for the influences on dust with different masses and sizes in our future papers.

As a galaxy evolves, $Q^*_{\rm pr}$ for a given grain also changes according to the time evolution of its SED. It is therefore self-consistent and ideal for the present study to estimate $Q^*_{\rm pr}$ at each time step by considering the SED evolution of a galaxy. However, this self-consistent estimation of time-varying $Q^*_{\rm pr}$ could make the present simulated code very complicated, because the derivation of the dust-corrected SED of a simulated galaxy is not a simple task (e.g., Bekki & Shioya 2000). We therefore adopt an idealized model in which $Q^*_{\rm pr}$ for a dust grain is constant all over the time in a simulation. We mainly investigate the evolution of disk galaxies with a smaller gas fraction only for ~ 1 Gyr for most models. Therefore, this assumption might be justified, because the SED does not change drastically owing to the lack of major bursts of star formation.

Barsella et al. (1989) derived $Q^*_{\rm pr}$ by assuming a single black body temperature and listed the values for different temperatures in their Table 1. F91 considered the SEDs of galaxies with Sb and Sc Hubble types and estimated $Q^*_{\rm pr}$ and showed the dependence of $Q^*_{\rm pr}$ on dust grain sizes in their Fig. 1. The estimated $Q^*_{\rm pr}$ of silicate with $R_{\rm dust} = 0.1$ μm is ~ 1 and that of graphite grains with $R_{\rm dust} = 0.05$ μm is ~ 1 too for late-type disk galaxies. Although we use these values as a reference, we also investigate how the present results depend on $Q^*_{\rm pr}$ by using the models with different $Q^*_{\rm pr}$.

2.14 Dust-related processes not included in this work

It is important for the present study to clearly indicate the dust-related physical processes that are not included in the new live dust particle model (Table 1 briefly summarize this). The following three important processes are not modeled in the present study. The first is the size distribution of dust and its evolution in ISM of galaxies. The dust size distribution, which is a key parameter for the SEDs of galaxies, can be significantly evolved owing to selective destruction of smaller dust grains (e.g., Asano et al. 2014). The second is the dust evolution due to coagulation and shattering of dust grains in ISM, which is included in recent one-zone models (e.g., Hirashita 2012). Given that the net formation efficiency of H_2 on dust grains in ISM of a galaxy depends strongly on the dust size distribution, not including these two could underestimate or overestimate H_2 contents of galaxies.

Third is the destruction of dust by warm/hot gaseous halos of galaxies, the detailed processes of which would depend on the mass-density and temperature of gaseous halos. This non-inclusion of dust destruction can result in the overestimation of the total dust mass in the halo regions of galaxies. The lack of the detailed observational information on the 3D distributions of gas density and temperature in the Galactic halo currently prevents us from discussing the level of this possible overestimation of the dust mass. Other possibly important factors, such as magnetic fields and turbulence of ISM, are not included either in this work, because they could play a relatively minor role in comparison with other factors discussed in the present work.

The size distributions of dust can be influenced by dust formation, destruction, growth, coagulation, and shattering processes, and thus SEDs can be influenced by these processes too. The radiation pressure of stars on dust grains is determined by $Q^*_{\rm pr}$ and thus by dust-corrected SEDs. Therefore, ultimately speaking, both (i) radiative-transfer of stellar light in dusty ISM and (ii) dust-related physical processes need to be self-consistently solved at each time step in a simulation. This means that the present code is not so fully self-consistent and our future simulation codes will need to incorporate above two complicated ingredients of dusty ISM evolution for modeling ISM of galaxies in a much more self-consistent way.

2.15 Parameter study

2.15.1 Fiducial MW-type disk galaxy model

We mainly investigate the MW-type disk model with $M_{\rm h} = 10^{12}{\rm M}_\odot$ in which spatial distributions of gas and stars are consistent with the observed one for the Galaxy. The adopted model parameters such as $M_{\rm s}$ and $M_{\rm g}$ are given in Table 4. Since the main purpose of this paper is not to describe the dependences of the results on the physical properties of disks, we investigate only three other disks models. These are 'LMC-type' (referred to as 'LMC') with $M_{\rm h} = 10^{11}{\rm M}_\odot$, 'Dwarf-type' ('DW'), with $M_{\rm h} = 10^{10}{\rm M}_\odot$, and 'Sa-type' with $M_{\rm h} = 10^{12}{\rm M}_\odot$ and a big bulge with $M_{\rm b} = 1.2 \times 10^{11}{\rm M}_\odot$ (i.e., B/T=0.67 corresponding to early-type spirals). These names are used just for distinguishing three disk galaxies with different $M_{\rm h}$. The model parameters for these disk models are also given in Table 3.

First we show the results of the fiducial MW-type disk model with stellar radiation pressure on dust grains in order to discuss the basic roles of the radiation pressure on dust evolution in §3.1. We do not include dust-related physical processes other than stellar radiation pressure in the fiducial model, because we need to show the basic roles of dust as clearly as possible. Then we describe how the present results can depend on other model parameters in §3.2. The basic parameters and physical processes included (or not included) in the fiducial model are given in Table 4. The initial total numbers of particles used in the fiducial MW-type, LMC-type, Dwarf-type, and Sa-type disk models are 1134000, 1100000, 1100000, and 1234000, respectively. The total particle numbers can increase as star formation creates new SNe and AGB stars.

2.15.2 Key parameters

The main purpose of this paper is to understand the roles of radiation-driven dust wind in the evolution of dust, star formation rates (SFRs), and molecular fractions ($f_{\rm H_2}$), and chemical abundances of galaxies. Therefore we first investigate these roles by using the fiducial MW models with and without radiation pressure of stars on dust. In these models, the effects of photo-electric heating, dust-gas heating, gaseous drag, and cosmic-ray heating are not included so that we can more clearly understand the roles of radiation-driven dust wind in galaxy evolution. The key parameters in this first study is the initial ages of stars in the disks (t_0), $Q^*_{\rm pr}$, dust-types, and $A_{\rm t}$ (total dust extinction). Then we investigate different disk models with and without different

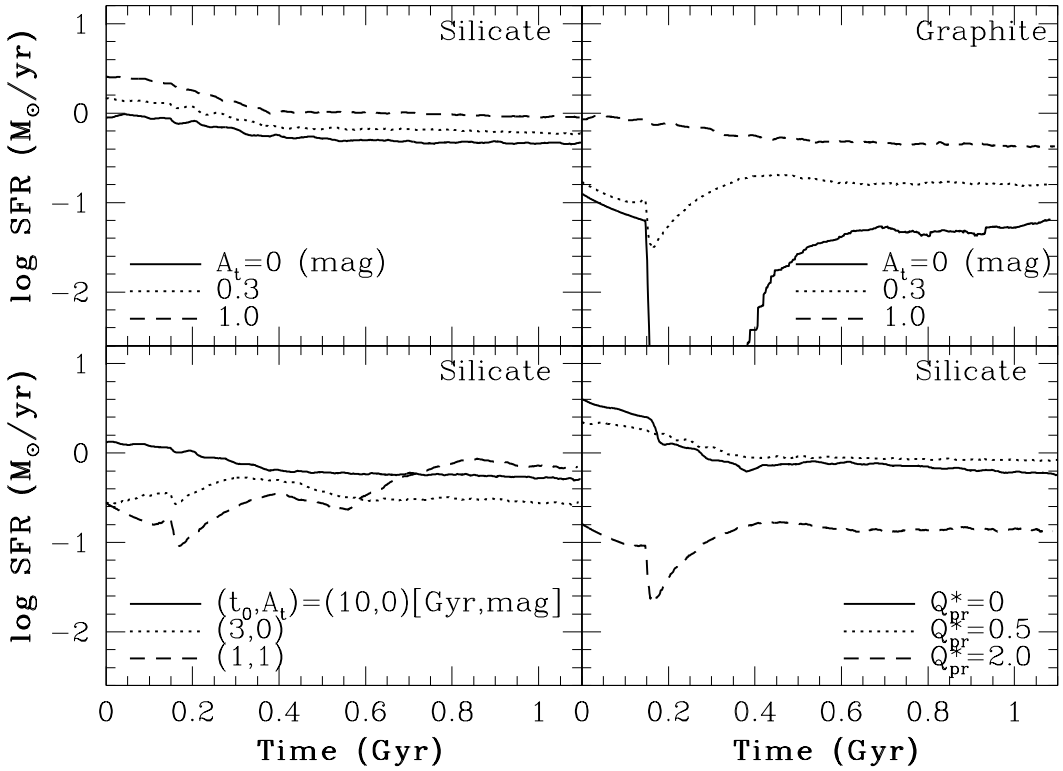

Figure 8. The time evolution of SFRs in the 12 representative models. The line types are exactly the same as those used in Fig. 5.

dust physical effects in order to confirm whether the roles of radiation-driven dust wind in galaxy evolution in these models can be clearly seen in the models. The adopted values of the four key parameters are shown in Table 5.

2.15.3 Photo-electric heating and gas-dust drag

Although we have found important roles of photo-electric heating of ISM by dust in the star formation histories (SFHs) of galaxies, we do not discuss these extensively in the present study, and will describe them in detail in our forthcoming papers. This is mainly because we need to discuss this issue thoroughly by using the results of many models and thus it is not so appropriate for the present study to include them in this first paper. We have also found the effects of gas-dust drag on the evolution of the 3D spatial distributions of gas and dust in galaxies. We however discuss these in our forthcoming paper for the same reason as above.

3 RESULTS

3.1 MW-type disk

3.1.1 Radiation-driven dust evolution

Fig. 1 shows how the strong radiation field of old stars in the disk can influence the dynamical evolution of old silicate in the fiducial MW-type disk model. Here 'old dust' means dust particles that are initially in the disk, and therefore the old dust particles do not include dust produced from SNe and AGB stars after star formation. Clearly, the inner dust particles can be pushed out by the galaxy-wide strong radiation pressure of stars so that a ring-like structure can be once formed in the disk ($T = 0.28$ and 0.56 Gyr). The initially thin disk of old dust appears to be thickened owing to the outward transfer of dust particle by the radiation pressure. The mean $|z|$ of the dust particles can increase from 0.24 kpc at $T = 0$ Gyr to 1.4 kpc at $T = 0.28$ Gyr to 1.9 kpc at $T = 1.1$ Gyr in this model. The final distribution of the old dust disk viewed from edge-on is like a disk galaxy with an inner thick disk ($T = 1.1$ Gyr).

Most of the dust particles can not escape from the galaxy owing to the deep galactic potential of this massive disk galaxy ($M_{\rm h} = 10^{12}{\rm M}_{\odot}$). Only 0.4% of the particles can once locate outside the virial radius ($r_{\rm vir} = 245$ kpc) and 98% of the particles are finally within $R_{\rm g}$ ($= 2R_{\rm s}$) (=initial gas disk size) in this model. However, as shown in Fig. 2 for the time evolution of the spatial distributions of graphite, a large fraction of graphite appears to escape from the inner halo region of the galaxy. About 19% of the particles can escape from the galaxy (i.e., $R > r_{\rm vir}$) within ~ 1 Gyr, and only 24% of the particles still can be within $R_{\rm g}$ at $T = 1.1$ Gyr. The mean $|z|$ of the dust particles can increase from 0.24 kpc at $T = 0$ Gyr to 24.5 kpc at $T = 0.28$ Gyr to 57.7 kpc at $T = 1.1$ Gyr for the graphite particles. These results confirm the earlier result (F91) that graphite can move faster than silicate and thus can escape from galaxies under the strong radiation pressure of stars.

The key factor that can control the dynamical evolution of dust in galaxies is the ratio (β) of radiation pressure force to gravitational one:

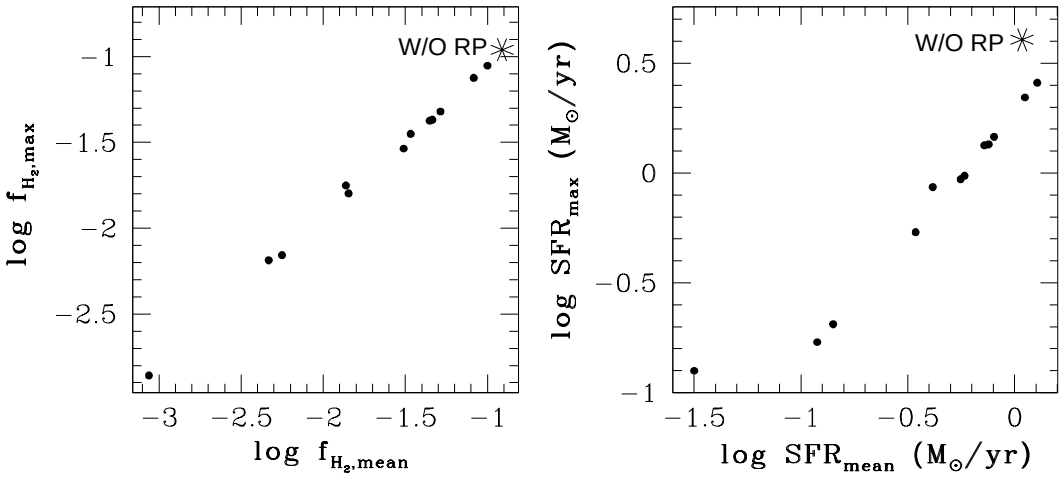

Figure 9. The plot of 12 representative models on the $f_{\rm H_2,mean} - f_{\rm H_2,max}$ (left) and $\rm SFR_{mean} - SFR_{max}$ (right) planes. Here $f_{\rm H_2,mean}$ and $\rm SFR_{mean}$ are the mean $f_{\rm H_2}$ and SFR over the 1.1 Gyr evolution, respectively, whereas $f_{\rm H_2,max}$ and $\rm SFR_{max}$ are the maximum values of $f_{\rm H_2}$ and SFR, respectively. For comparison, the models without dust-related physics is shown as 'W/O RP' (without radiation pressure).

$$\beta = \frac{F_{\rm rad}}{F_{\rm grav}}. \tag{36}$$

This β parameter is different between silicate and graphite because it depends on the adopted different dust mass densities and sizes:

$$\beta \propto R_{\rm dust}^2/m_{\rm dust} \propto R_{\rm dust}^{-1}\rho_{\rm dust}^{-1}. \tag{37}$$

Therefore, the β value is larger for graphite for the adopted $\rho_{\rm dust}$ (lower for graphite) and $R_{\rm dust}$ (smaller for graphite) so that graphite can be more strongly influenced by radiation pressure of stars in galaxies.

As a result of radiation-driven dust transfer, the radial density profiles of these dust particles can change significantly within the ~ 1 Gyr dynamical evolution of the disk. Fig. 3 shows that the final distribution of the silicate particles at $T = 1.1$ Gyr is more flattened than the initial exponential profile adopted in this model. The final distribution for the inner halo region $R \sim 20 - 30$ kpc is more similar to the observed profile of dust ($\Sigma_{\rm dust} \propto R^{-0.8}$) by Ménard et al 2010 (M10). The final profile of the graphite particles within the inner halo region is even more flattened and therefore very similar to the observed flat profile of dust (M10). These results strongly suggest that the spatial distributions of many different dust species can be heavily influenced by radiation pressure of stars in galaxies. Furthermore, given that our previous simulations without radiation pressure of stars (B13a) failed to explain the observational results by M10, these results imply that the origin of the very flat distribution of halo dust can be closely related to the exertion of stellar radiation pressure on dust grains.

As shown in Fig. 4, the newly produced silicate particles (i.e., SNIa, SNII, and AGB dust) do not clearly show the flattened density profiles at the selected three time steps. One reason for this is that these dust particles are born in the very thin gas disk (at small $|z|$), where the dust particles can not be levitated to a great extent by stellar radiation pressure owing to the deeper gravitational potential. The other reason is that these 'younger' particles have not had enough time to travel to the outer halo region at $T = 1.1$ Gyr. These results imply that there could be some differences in the spatial distributions of dust grains that were formed in a galaxy at different epochs. The mass fraction of silicate that can escape from the galaxy within 1.1 Gyr evolution is 0.0007 for SNIa, 0.0012 for SNII, and 0.0002 for AGB. The final mean $|z|$ for SNIa, SNII, and AGB dust are 1.4, 1.5, and 1.3 kpc, respectively. It is interesting to note that the vertical distribution of SNII dust is slightly thicker than those of other dust types.

The derived outward transport of dust in the disk suggests that radiation pressure of old disk stars can flatten the radial gradients of D. Furthermore, this outward transport could be a new mechanism of metal-enrichment process in the very outer parts of galactic gas disks, if dust can be destroyed and then returned back to ISM there. The ejection of dust into the outer halo region of a galaxy means that both the mean D and dust-to-metal-ratio ($D_{\rm z}$) of the gas disk of the galaxy can be lowered significantly. The observed large scatter in D for a given gas-phase abundance (e.g., Galametz et al. 2011) could be also closely associated with this dust ejection process. Since this radiation-driven dust wind is not considered in previous one-zone chemical evolution models with dust (e.g., D98; Inoue 2003), D and $D_{\rm z}$ evolution would need to be re-investigated in future one-zone models for dust evolution.

In the present simulations, the mass of each dust particle ($m_{\rm d}$) is rather small in comparison with those of other components (DM, stars, and gas). For example, the initial mass of an old dust particle in the fiducial MW-type disk model is only 0.6% (0.06%) of the gas (star) particle mass ($m_{\rm d} = 3.6 \times 10^2$ $\rm M_\odot$). The mass-ratio of dust to gas (star) can also become rather small for newly formed SNIa, SNII, and AGB dust particle, because (i) the masses of these dust particles are only small portions of their parent gas particles and (ii) the significant fraction of dust can be consumed by star formation and destroyed by SNe.

However, $m_{\rm d}$ can become much larger than their initial

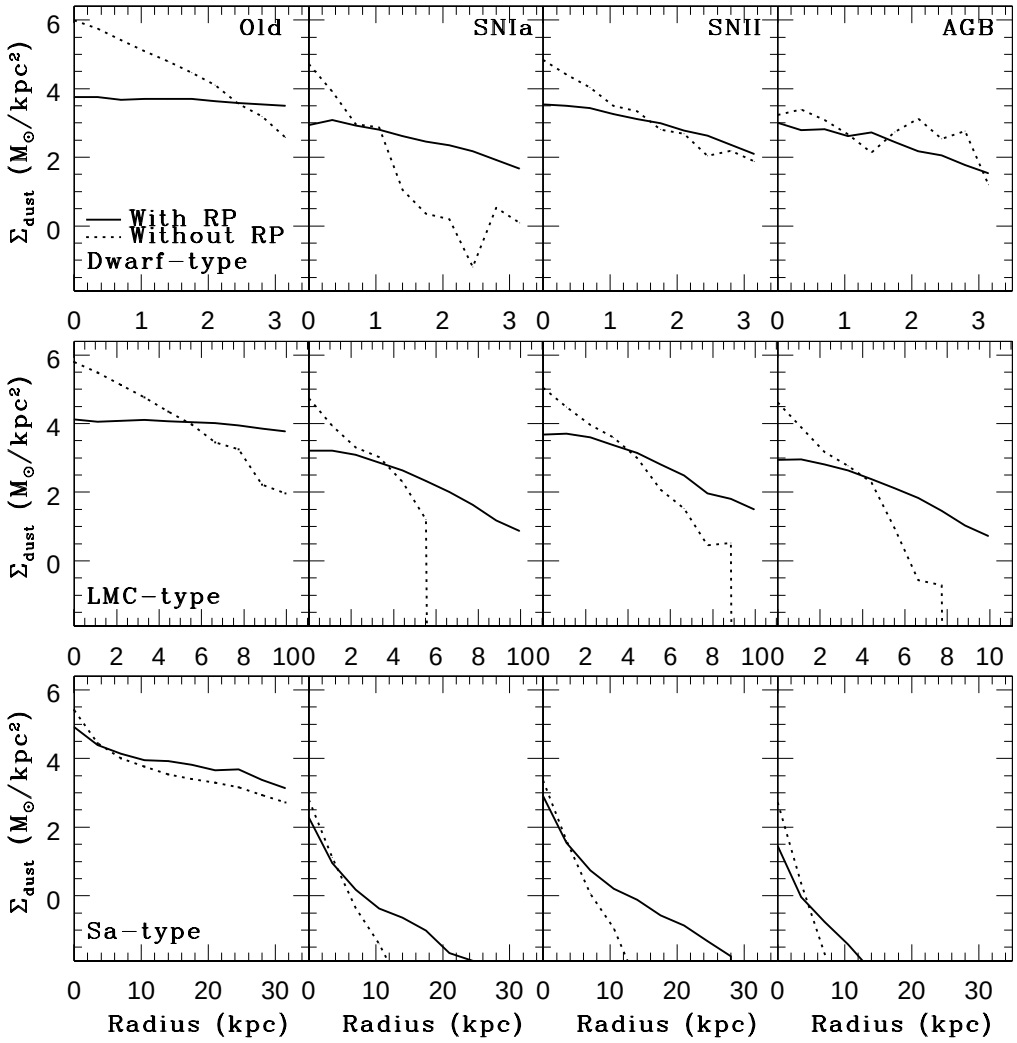

Figure 10. The final projected radial density profiles of silicate for old (left), SNIa (second from the left), SNII (second from the right), and AGB (right) for the models with (solid) and without (dotted) radiation pressure (RP). The top, middle, and bottom panels show the results for Dwarf-type, LMC-type, and Sa-type galaxy models, respectively. The profile for $R \leqslant R_{\rm g}$, where $R_{\rm g}$ is the initial gas disk size of a galaxy, is shown for each model.

values in some local regions owing to dust growth. Accordingly, the mass range of dust particles can be quite large in a simulation. For example, $m_{\rm d}$ for SNII dust can range from 3.8×10^{-1} $M_\odot$ to 1.9×10^3 $M_\odot$ for the fiducial MW disk model. The average $m_{\rm d}$ for SNII dust produced during ~ 1 Gyr evolution of the MW model is 1.8×10^2 $M_\odot$, and the above very low-mass SNII dust particle is very rare. In spite of this large mass difference, the gravitational softening length is fixed at a same value among all baryonic components.

This means that the dust particles could be dynamically heated up (i.e. have more randomized motions) after they encounter with much more massive stellar and gaseous (and dark matter) particles. Although this possible heating of dust particles can be an undesired numerical artifact in the present study, such a dynamical heating (e.g., the formation of very thick dust disk) can not be clearly seen in an isolated MW-type disk model. Therefore, it is safe for us to conclude that the transfer of dust to the outer halo regions shown in Figs. 1 and 2 are due to the effects of radiation pressure on dust (not due to the numerical heating caused by particles with vastly different masses).

It should be also noted here that the dust destruction by warm/hot halo gas in galaxies is not included in the present simulations. This means that the extension of dusty halo caused mainly by radiation pressure of stars might be overestimated. Dust moving fast in the warm/hot gaseous halo of a galaxy might be destroyed efficiently (e.g., F91, Bianchi & Ferrara 2005) so that the total mass of dust in the galactic halo can be reduced significantly. As a result of this, the outer profile of the dust mass density become steeper in the model with dust destruction by the gaseous halo. This possible effect of gaseous halos of galaxies on dust will need to be investigated in detail by our future studies.

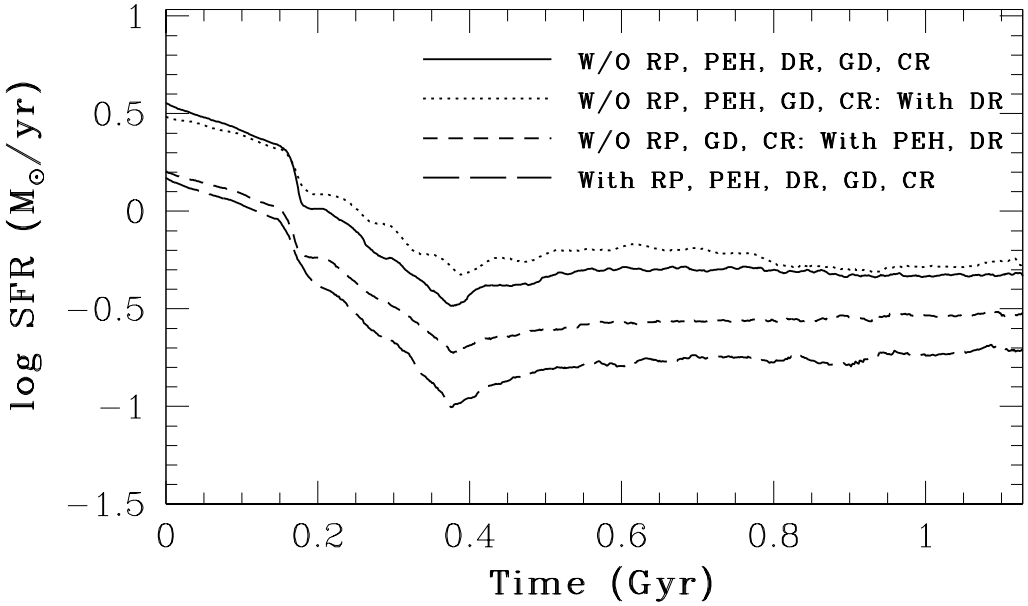

Figure 11. The time evolution of SFRs in the MW-type disk models with or without dust-related physical processes: without any dust-related processes (solid), with DR and without ('W/O') RP, PEH, GD, and CR (dotted), with PEH and DR and without RP, CR, and GD (short-dashed), and with PEH DR, RP, CR, and GD (long-dashed),

3.1.2 The roles of $A_{\rm t}$, t_0, and $Q^*_{\rm rp}$ in dust evolution and SFH

Fig. 5 describes how the final projected density profiles of old dust particles at $T = 1.1$ Gyr in the inner halo region (< 30 kpc) for the MW-type disk model depend on the adopted A_t (total dust extinction), dust types (silicate or graphite), initial stellar ages of old disk stars (t_0), and frequency-averaged radiation pressure coefficient ($Q^*_{\rm pr}$). Firstly, the models with larger $A_{\rm t}$ show steeper radial profiles of silicate, mainly because the higher degrees of dust extinction severely weakens the stellar radiation pressure on dust so that the spatial distribution of dust can not change significantly. This dependence can be clearly seen in the models with graphite, though the distribution of graphite is more flattened than that of silicate for all models with different $A_{\rm t}$. Secondly, the models with younger ages of old stars in disks show flatter density profiles of dust: this is confirmed to be true for graphite. The reason for this is that the stronger radiation pressure of younger stars in a disk can cause the efficient radial transfer of dust to the outer region of the disk.

Thirdly, the models with larger $Q_{\rm pr}$ show flatter radial profiles of dust, because dust with larger $Q_{\rm pr}$ can be more strongly influenced by stellar radiation pressure. The outer radial profiles of dust and $f_{\rm esc}$ also depend on $A_{\rm t}$, dust types, t_0, and $Q^*_{\rm pr}$. For example, $f_{\rm esc}$ for graphite in the MW model with $A_{\rm v} = 0.3$ mag is 0.07, which is about 35% of the same model with $A_{\rm t} = 0$ mag (shown in Fig 2). Fig. 6 describes the time evolution of the spatial distribution of graphite for the MW model with $A_{\rm t} = 0.3$ mag. In spite of reduced stellar radiation pressure, some fraction of dust particles still can escape from the galaxy to locate outside $r_{\rm vir}$ at $T = 1.1$ Gyr. The final slope of the flattened density profile at $R > 50$ kpc appears to be rather similar to the observed one by M10, which again suggests that the origin of the observed flat dust distribution can be caused by radiation-driven dust wind.

Fig. 7 describes the time evolution of the spatial distribution of silicate for the MW model with a larger dust extinction ($A_{\rm t} = 1$ mag) and radiation pressure. Although the outer distribution of dust is rather flattened owing to the outward transfer of dust, the flattening is due largely to the extended disk of dust. The dusty wind to the vertical direction can not be clearly seen in this model, because the dust extinction of stellar light by the dusty disk can weaken the stellar light and thus prevent the radiation pressure from pushing out dust particles to a large extent. This derived importance of $A_{\rm t}$ implies that the levels of dust extinction dependent on local properties of ISM need to be more self-consistently modeled so that dust dynamics driven by stellar radiation pressure in galaxies can be more self-consistently investigated in our future studies.

Since the dust surface densities of disk galaxies can change significantly owing to the radiation-driven dust wind (or dust levitation), the formation efficiency of H_2 ($\epsilon_{\rm H_2}$) on dust grins can also evolve with time. The severe reduction of dust mass densities in disks results in lower $f_{\rm H_2}$ in most models with non-zero $Q^*_{\rm pr}$ in the present study. The lower $f_{\rm H_2}$ means lower SFRs in the disks, because the present study adopted the H_2-dependent SF recipe. Fig. 8 demonstrate how the SFHs of disk galaxies can be influenced by strong radiation pressure of stars in the 12 MW-type disk models with different parameters. The following five key parameter dependences are found for these representative models.

Firstly, the models with smaller $A_{\rm t}$ show systematically lower SFRs, because stronger radiation fields can lower the dust mass densities of the disks and thus more severely suppress star formation in H_2 gas clouds. Secondly, the models

with graphite show lower SFRs than those with silicate, because graphite can be more strongly influenced by radiation pressure of stars so that the mass densities of graphite in the disks become lower. The dependence of SFRs on $A_{\rm t}$ found in the models with silicate can be clearly seen in the models with graphite. Thirdly, the models with younger ages of old stars in the disks show lower SFRs for a given $A_{\rm t}$. The model with $(t_0, A_{\rm t})$=(1,0) [Gyr, mag] is not shown in this figure, because SFR becomes almost 0 in the model even from the early stage of disk evolution, because almost all dust is expelled from the disk owing to the very strong radiation pressure of young stars. The young disk model with more severe dust extinction, i.e., $(t_0, A_{\rm t})$=(1,1) [Gyr, mag], shows lower SFRs in the early stage of disk evolution ($T < 0.6$ Gyr), which implies that star formation can be severely suppressed by radiation pressure in young disk galaxies at high z. It is interesting that the model shows higher SFRs at later times when the radiation field becomes much weaker and the disk still has a plenty of gas.

Fourthly, SFRs can become lower in the model with $Q^*_{\rm pr} = 2.0$ than $Q^*_{\rm pr} = 0.5$, because dust is more efficiently removed from the thin disks in the model with larger $Q^*_{\rm pr}$ so that H_2 mass densities can become lower too. The model with $Q^*_{\rm pr} = 0$ corresponds to no radiation pressure, and accordingly this model shows the highest SFRs at $T < 0.2$ Gyr among the 12 models. Owing to the more rapid H_2 consumption by star formation at $T < 0.2$ Gyr, this model shows lower SFRs in later times. These results in Fig. 8 clearly demonstrate that (i) radiation pressure on dust grains can reduce SFRs in galactic disks and (ii) the level of this SFR reduction (and H_2 formation efficiencies on dust grains) depends on the physical parameters of the disks and dust. Fig. 9 summarizes the levels of SFR and $f_{\rm H_2}$ reduction due to stellar radiation pressure on dust grains for the 12 representative models. Clearly, both the mean and maximum $f_{\rm H_2}$ and SFR can become lower in the models with radiation pressure.

In real disk galaxies, their interstellar dust is composed of dust grains with different compositions and sizes. Furthermore, the ages of old populations in a disk galaxy should be quite diverse depending on its formation history and thus can not be represented by a single age. Accordingly, the above models with a single t_0 and either only silicate or only graphite would be rather idealized and less realistic. Therefore it should be stressed here that the 12 models are used for illustrating the possible effects of radiation pressure on SFHs of galaxies. We will discuss how radiation pressure of stars can influence galaxy-wide SFHs and H_2 evolution in a more convincing manner by using a galaxy formation model based on ΛCDM model in our forthcoming papers.

3.2 Other models

3.2.1 Low-mass disk models

It is confirmed that the influences of stellar radiation pressure on dust distributions, $f_{\rm H_2}$ evolution, and SFHs derived for the MW-type disk models are seen also in the LMC-type and Dwarf-type low-mass disk models. Accordingly, we briefly describe the results of these models here. The evolution of dust distributions in these low-mass disks can be more strongly influenced by radiation pressure of old stars owing to the shallower gravitational potential. Fig. 10 clearly demonstrates that all dust components (old, SNIa, SNII, and AGB) in the LMC-type disk model with radiation pressure show flatter radial density profiles in comparison with the model without radiation pressure. The old dust have a flatter final distribution than other dust components, which is seen in the MW-type disk model too.

As shown in Fig. 10, these important roles of radiation-driven dust wind found in the LMC-type disk models can be clearly seen in the Dwarf-type disk models, though the difference of AGB dust distributions between the models with and without radiation pressure is less clear. The less clear flattening of dust distribution for AGB dust is due to the later formation of dust in these models with rather low SFRs. These results imply that the present result on the key role of stellar radiation pressure on the evolution of dust distributions in galaxies can be universal among galaxies with different masses. These also suggest that the halos of low-mass disk galaxies can contain a large amount of dust owing to dust wind driven by stellar radiation pressure, if the possibly warm halo gas can not destroy the ejected dust so efficiently.

3.2.2 Massive bulge models

Fig. 10 shows that the massive bulge model (Sa-type) with stellar radiation pressure have flatter density profile of dust for all dust components. However, the slopes are not so flat as those derived for the LMC- and Dwarf-types disk models, because the deeper gravitational potential of the massive bulge can prevent dust from escaping from the thin disk. Massive bulges in disk galaxies can suppress the formation of molecular hydrogen in spiral arms (B14), because they can stabilize the disks against gravitational instability (no formation of strong spirals and bars). Therefore, star formation can be suppressed, and the total amount of dust can not rapidly increase. The systematically lower dust mass densities in these models are due largely to the low production rate of dust caused by lower SFRs. These results combined with those in the MW-type disk models imply that the 3D distributions of dust in galactic halos could be different in galaxies with different Hubble types.

3.2.3 Other dust effects

We have so far focused on the results of the models that do not include dust-related physics (e.g., photo-electric heating and dust destruction by SNe) other than stellar radiation pressure on dust grains. This is mainly because our main purpose is to investigate how the stellar radiation pressure, which is not included in B13a, can possibly influence galaxy evolution. The influences of other each dust-related physics on galaxy evolution will be separately discussed in our forthcoming papers. Although photo-electric heating (PEH), cosmic-ray heating (CR), dust-gas heating (DG), gaseous drag of dust (DR), and dust destruction can influence the thermal history of gas and dust, they can not change the evolution of the 3D dust distribution so dramatically than stellar radiation pressure (RP): this is indeed confirmed in the present study.

The essential role of stellar radiation pressure on dust

evolution can be seen in the models with RP, PEH, CR, DR, DG, and dust destruction. The suppression of H_2 formation and star formation by radiation pressure of stars can be seen in these models, though other dust-related physics can significantly modify the suppression effects. Fig. 11 shows a number examples of key effects of these dust-related physics on SFHs of disk galaxies. The gaseous drag (DR) in the model without RP yet with DR can prevent dust particles from escaping from the thin gas disk where star formation can occur so that the SFR can be slightly higher in the model than in the model without RP and DR. The model with PEH shows a systematically low SFR owing to the increased gaseous temperature (in particular for $T < 10^4$ K) of cold ISM. This suppression of SF by PEH can be seen in the models with or without RP, which implies that PEH can play a key role in SFHs of galaxies. This role of PEH should be extensively explored in our future works.

As shown in Fig. 11, the model with all dust-related physical processes shows the lowest SFR among the four models. This implies that if numerical simulations of galaxy formation and evolution do not include dust physics properly, then they could severely overestimate the galaxy-wide SFRs. Given that such dust effects on galactic SFHs can be stronger in galaxies with lower masses, the results in Fig. 11 implies that the total stellar masses of low-mass disk galaxies could have been overestimated in the previous simulations of galaxy formation without dust. It should be stressed that these discussion on galactic SFHs is based on the adopted H_2-dependent SF models. If SFRs are simply proportional to total gas densities (neutral + molecular hydrogen), then the influences of dust-related physics on SFHs could be reduced to a large extent, because SFRs do not depend on the H_2 evolution that is strongly influenced by dust evolution.

4 DISCUSSION

4.1 How can galactic chemical evolution be possibly influenced by dust evolution?

The chemical evolution of galaxies can be influenced largely by their SFHs that are controlled by a number of physical processes, such as merging histories of galaxies, stellar winds by energetic feedback effects, and molecular cloud formation. Given that dust grains are the major formation sites of H_2 gas in galaxies, the evolution of dust abundances, compositions, and sizes can be a key factor for H_2 evolution and thus for chemical evolution of galaxies. Although a full investigation of this issue should be done in our future studies with the present new code, it would be instructive for the present study to discuss the possible influences of dust evolution in galactic chemical evolution briefly. Fig. 12 shows the time evolution of gas-phase metal abundances ($Z_{\rm g}$), metal abundances of new stars ($Z_{\rm ns}$), dust-to-gas-ratios (D), and dust-to-metal-ratios ($D_{\rm z}$) for the MW-type models without radiation pressure ('W/O RP') and different $f_{\rm dest}$. For comparison, the results of the model without dust growth and destruction are shown in this figure.

Clearly, the evolution of $Z_{\rm g}$, $Z_{\rm ns}$, D, and $D_{\rm z}$ depends strongly on how much fraction of dust can be destroyed by SNe in a star-forming cloud. In the model with $f_{\rm dest} = 0.03$, a larger fraction of dust can be returned back to ISM as gas-phase metals owing to the more efficient dust destruction so that gas-phase metallicity ($Z_{\rm g}$) can increase more rapidly and to a larger extent. Because of the higher gas-phase metallicity of the ISM, the new stars can also have higher metallicities ($Z_{\rm ns}$). As a result of this, D and $D_{\rm z}$ can decrease with time in this model with higher $f_{\rm dest}$. On the other hand, the model with low $f_{\rm dest}$ (=0.01) shows slower increase in $Z_{\rm g}$ and $Z_{\rm ns}$ and significant increase in D and $D_{\rm z}$. These results suggest that dust destruction by SNe in ISM can greatly influence the chemical evolution of galaxies.

As shown in the present study, the stellar radiation pressure can levitate dust to the halo regions of galaxies where gas densities are so low that dust can not efficiently grow. The radiation pressure also can suppress the galaxy-wide star formation and consequently slow down the chemical enrichment processes of galaxies. Therefore, the stellar radiation pressure on dust can influence the time evolution of $Z_{\rm g}$, $Z_{\rm ns}$, D, and $D_{\rm z}$. Fig. 13 clearly demonstrates that $Z_{\rm g}$ and $Z_{\rm ns}$ can more slowly increase with time in the models with RP. Although the model with a low $f_{\rm dust}$ (=0.01) shows a slow increase in D, it shows a slight decrease of $D_{\rm z}$. In this model, gas-phase metallicity can steadily increase due to star formation, because ISM can not be so efficiently ejected into the halo region. However, dust-phase metallicity can not increase so efficiently through accretion of gas-phase metals onto dust grains, because a significant fraction of dust can be ejected into the halo region where gas density is low Therefore, the destruction of dust by SNe can lower $D_{\rm z}$ even in this model with low $f_{\rm dest}$.

Thus, these results suggest that we need to carefully model the dust-related physics in ISM of galaxies in order to discuss the chemical evolution of galaxies. One of the most important parameters in the present new model is $f_{\rm dest}$, which needs to be determined by another sets of pc-scale simulations of forming and evolving molecular clouds with young stars and SNe. Since $f_{\rm dest}$ is defined for an entire star-forming cloud with multiple SNe, we can not simply use the results of simulations for dust destruction by a single SN event (e.g., Nozawa et al. 2003). Given that $f_{\rm dest}$ can so strongly influence the time evolution of dust and metal abundances, it is doubtlessly our future study to determine the reasonable range of $f_{\rm dest}$ for galaxy-scale simulations. The best way to do so would be to compare the observed scaling relation of dust properties (such as a D-$Z_{\rm g}$ relation, e.g., Galametz et al. 2011) the corresponding simulations with different $f_{\rm dest}$. It would be also necessary for our future theoretical works to search for the possible range of $f_{\rm dest}$ and its dependence on ISM properties based on sub-pc-scale simulations of star-forming molecular clouds.

4.2 Galaxy life slowed down by dust

The present study has first shown that the radiation pressure of stars on dust can suppress the galaxy-wide star formation, because the pressure can reduce the H_2 mass fractions that can control SFRs of galaxies. This suggests that radiation-driven dust wind can change the chemical evolution of disk galaxies not only through the removal of some metals in the disks (Bekki & Tsujimoto 2014) but also through 'slowing down' the gas consumption by star formation thus the chemical enrichment processes. Accordingly, the present study implies that this 'slowed down' lives of galaxies could be

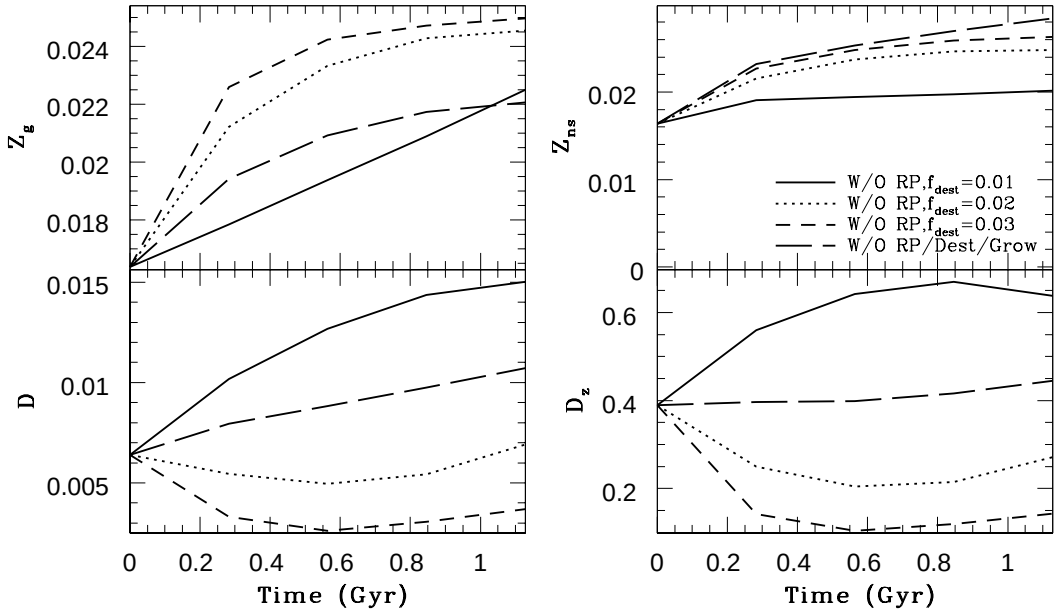

Figure 12. The time evolution of mean gas-phase metallicity ($Z_{\rm g}$, upper left), mean metallicity of new stars ($Z_{\rm ns}$, upper right), dust-to-gas-ratio (D, lower left), and dust-to-metal-ratio ($D_{\rm Z}$, lower right) for the four MW-type disk without stellar radiation pressure. Silicate is adopted for the dust component. The solid, dotted, and short-dashed lines indicate the models with different $f_{\rm dust} = 0.01$, 0.02, and 0.03, respectively. For comparison, the results for the model without dust growth and destruction are shown by a long-dashed line. Since there is no new star at $T = 0$, the initial $Z_{\rm g}$ value is plotted for $Z_{\rm ns}$ at $T = 0$.

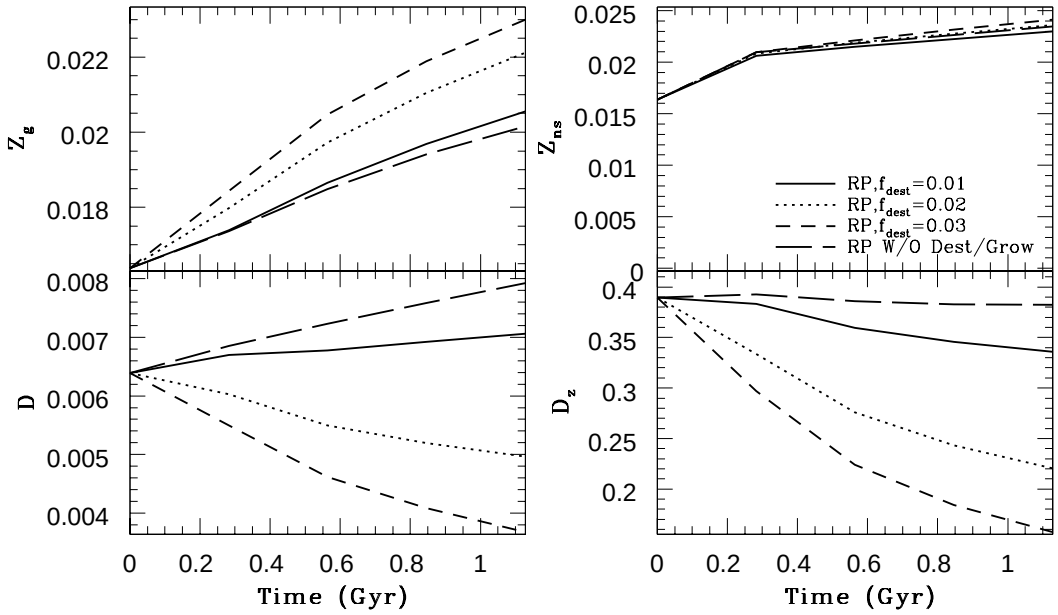

Figure 13. The same as Fig. 12 but for the MW-type disk model with stellar radiation pressure.

one of key results of galaxy formation and evolution influenced by interstellar dust. The present study also suggests that if numerical simulations of galaxy formation and evolution do not include dust-related physical processes in a self-consistent manner, then they are likely to over-predict the total gas mass converted into new stars.

The present study, however, has shown that the level of SF suppression by radiation-driven dust wind depends on the adopted constant dust extinction of ISM and the dust composition. This implies that our future more sophisticated models with a self-consistent model for radiative-transfer of stellar light in dusty ISM (which can properly predict $A_{\rm t}$ variation in time and space) would produce different results. Furthermore, the SF suppression can be clearly seen in the present simulations, because SFRs are assumed to depend on the mass densities of H_2 the formation efficiency

of which depends strongly on dust densities. Accordingly, if SFRs depend on the total gas densities rather than H_2 densities, then the SF suppression would not be so clear as the present models have shown. Thus, the level of SF suppression by radiation-driven dust wind needs to be investigated by our more sophisticated models with a fully self-consistent treatment of stellar light influenced by local dust.

The possible influences of dust on galaxy formation and evolution revealed by the present study are summarized in Table 6. Given that the present new model is still idealized and less realistic in some points (e.g., non-inclusion of dust size distributions), these possible influences might be modified (at least in a quantitative sense) in more sophisticated models for dust formation and evolution in galaxies. Furthermore, the present simulations are only for disk galaxies in an isolated environment without no dynamical and hydrodynamical interaction with other galaxies. Some unknown influences of dust on galaxy formation would be likely to be found in numerical simulations of galaxy formation. Therefore, such influences of dust need to be re-investigated thoroughly in future numerical simulations of galaxy formation with a self-consistent modeling of dust-related physical processes in ISM.

4.3 Future directions of the new live dust particle method

The present new four-component chemodynamical code will enable us to investigate various aspects of dust-affected galaxy formation and evolution across the comic time. The proposed live dust particle method will make it possible for us to discuss the different distributions of gas and dust in galaxies, the cosmic evolution of dust sizes and compositions, and the abundances of interstellar matters formed on dust grains. Below, we briefly discuss what we can investigate by using the new simulation code (The figure in Appendix C would be useful for readers of this paper to understand the following discussion better).

4.3.1 Dust-gas decoupling

B15 failed to reproduce the observed flat profiles of dust halos of galaxies (M10), because the model adopted in B15 did not include dust-gas decoupling processes in ISM (e.g., radiation pressure and dust-gas drag). Furthermore, the observed rather high dust-to-gas-ratio ($D \sim 0.05$, which is about 6 times larger than the solar neighborhood) in the outer halo of M81 by Xilouris et al. (2006) was very difficult to be explained by B15 for the same reason. As shown in this paper, the radial density profile of dust in a galaxy can be flattened by the effects of radiation pressure of stars (thus the outer halo can have higher D). Therefore, it is doubtlessly worthwhile for our future studies to investigate whether such an important effect of radiation pressure can be clearly achieved in cosmological hydrodynamical simulations of galaxy formation.

4.3.2 Dust size distribution

The present chemodynamical model includes the six key dust-related physical processes of galaxies, i.e., dust formation, mixing, growth, destruction, consumption, and catalysis. The formation of H_2 on dust grains is one of important interstellar chemistry processes on dust grains ('catalysis') that can be discussed in the present study. The present new live dust particle method combined with the proposed four-component galaxy model (DM+stars+gas+dust) can predict dust and gas 3D distributions separately and distributions and kinematics of different dust species (e.g., AGB and SN dust) separately too. However, the live particle method is still less realistic in modeling some aspects of dusty ISM, such as the size evolution of dust and the coagulation process of dust.

The bottleneck of the new method is that the total number of dust particles can endlessly increase if the formation of dust with different sizes and components in star-forming regions and evolved stars is considered in a fully self-consistent manner. This means that the CPU/GPU time required for the calculation of dust physics at each time step of a simulation can become progressively longer as the simulation proceeds. The total number of dust particles ejected from a single stellar particle ($N_{\rm ej}$) is 3 in the present study so that the total number of particles (N) can not dramatically increase. However, if we investigate the time evolution of dust sizes, $N_{\rm ej}$ would possibly need to be more than ~ 100 to represent a statistically enough sample of dust grains with different sizes. This means that we need to develop a fast algorism for calculating the dust-related physics of ISM in a simulation in order to consider the dust size evolution in a self-consistent manner.

4.3.3 Self-consistent SED construction

Constructing the SEDs for arbitrary 3D geometries of gas, dust, and stars in galaxies based on theoretical and numerical models of galaxy formation has been one of key ares of theoretical studies of galaxies (e.g., Bekki & Shioya 2000, 2001; Jonsson 2006; Popescu & Tuffs 2013). These simulated SEDs and those based on some phenomenological models (e.g., Dale et al. 2001) are very useful in interpreting the observed energy budgets (e.g., fraction of infrared light) of dusty star-forming galaxies. In order to estimate SEDs from SSPs (e.g., Bruzual & Charlot 2003), the previous studies needed to assume (i) dust-to-metal-ratios (to drive dust abundances from gas metallicities) and (ii) dust size distribution (for deriving the dust extinction curves). If our future simulations with the new live dust particle method can predict dust size distributions properly, then they do not have to adopt the above assumption (ii) (the above (i) is explicitly derived in the present code already). Thus, the self-consistent construction of SEDs based on dust size evolution will be possible in our future studies.

4.3.4 Dust-corrected cooling

Although the gas-phase metallicity (that does not include dust-phase metal) of a gas particle should be used for estimating the radiation cooling rate of the gas in numerical simulations of galaxy formation and evolution, the total ISM metallicity (i.e., gas-phase + dust-phase metal) has been used in almost all simulations for cooling estimation, because dust was not included in the simulations. Al-

Table 6. A list of possible influences of dust on galaxy formation and evolution based on the present results. These need to be re-investigated thoroughly in future theoretical studies based on numerical simulations of galaxy formation and evolution with dust-related physics.

Dust-related physical processes	Galactic properties	Possible influences
Radiation pressure on dust (RP)	Dust distribution	Flattening of radial profiles and formation of outer dusty halos
	Gas dynamics	Less efficient H_2 cooling in ISM with lower T_g
	Star formation	Suppression of galaxy-wide star formation
	H_2 content	Reduction in thin gas disks
	Chemical enrichment	Slowed down metal-enrichment
Photo-electric heating (PEH)	Star formation	Significant suppression of galaxy-wide star formation
	H_2 content	Reduction in thin gas disks
Gas-dust drag (DR)	Dust distribution	Prevention of dust from escaping from galaxies
	Star formation	Mitigation of the RP's suppression effects of star formation

though the present new model properly considered this dust-corrected cooling process, it did not include the possible time-dependent IMF, which can cause significant changes in dust evolution, star formation histories, and chemical evolution of galaxies (e.g., Bekki 2013b; Recchi & Kroupa 2015).

Furthermore, the present study did not consider the radiative cooling rates that depend on both [Fe/H] on [Mg/Fe] (De Rijcke et al. 2013) thus on the detailed chemical evolution of galaxies. Given that the dust-depletion levels are quite different between different elements (e.g., Mg, Fe, and Ca), the present results might be changed to some extent if the cooling rates by De Rijcke et al. (2013) are adopted. Thus our future studies will need to include both temporal and spatial variations of IMFs and more sophisticated cooling models (De Rijcke et al. 2013) in order to model the thermal and dynamical evolution of ISM regulated dust in a more self-consistent way.

4.3.5 Dust destruction by multiple SNe

The present study has introduced a new parameter for the mass fraction of dust destroyed by SNe ($f_{\rm dest}$). In the simulation code, the dust particles that are within less than $R_{\rm dest}$ ('destruction radius') from a SN are assumed to be destroyed and consequently lose some fraction ($f_{\rm dest}$) of dust. Since a cluster of stars is formed from a gas particle, the previous results based on a model for dust destruction by a single SN can not be simply used in the present model. Given that $f_{\rm dest}$ can control chemical evolution of galaxies, the possible range of $f_{\rm dest}$ in star-forming gas clouds with multiple SNe exploding at different epochs needs to be investigated in our future simulations.

The mixing radius ($R_{\rm mix}$) of ejected metals from SNe and AGB stars and the dust destruction radius ($R_{\rm dest}$) are set to be the same in the present study. The appropriate values for $R_{\rm mix}$ and $R_{\rm dest}$ are determined from the adopted spatial resolution of a simulation (i.e., from $\epsilon_{\rm g}$). However, these two could be significantly different, because dust destruction processes might be more sensitive to physical properties of ISM (e.g., magnetic fields and gas shock speed; Jones et al. 1994). This means that we need to perform high-resolution sub-pc scale numerical simulations on the dynamical evolution of dust and metals ejected from SNe and AGB stars in galactic potentials. The outputs from such simulations will be able to be included in larger galaxy-scale simulations so that we can investigate the dust-regulated galaxy formation and evolution for reasonable ranges of $R_{\rm mix}$ and $R_{\rm dest}$.

4.3.6 Physical properties of interstellar ice and organic matter

Although we have so far focused on the formation of H_2 on dust grains, the surface of grains in ISM is crucial for the formation and evolution of many different interstellar species (as 'catalysis'), such as ice and organic matter (e.g., Herbst & van Dishoeck 2009). Accordingly, the present new dust particle methods will enable us to predict the formation efficiency of many different species other than H_2 by considering physical conditions of gas and dust and chemistry on dust grains. As a dust particle moves in ISM of a galaxy, the dust temperature, the collision rates of atoms and molecules, the strength of ISRF, and other physical properties of dust and ISM can change. If these time evolution of the physical properties of the dust and its environments can be investigated by our future simulations, we will be able to predict the time evolution of interstellar species (e.g., organic matter). Given that recent infrared observations have already shown different abundances of H_2O and CO_2 ices in different galaxies (e.g., Shimonishi et al. 2010), this prediction is something that we should do not in far future but in near future, though the modeling of H_2O and CO_2 ices might be a formidable task.

5 CONCLUSIONS

We have developed a new four-component model of galaxy evolution in which a galaxy consists of dark matter, stars, gas, and dust. The dust component is represented by 'live' dust particles so that the present new model enables us to investigate separately the evolution of gas and dust.The dust particles are 'live' in the following three senses. Firstly, dust particles can gravitationally interact not only with other components (e.g., dark matter) but also with other dust particles. Secondly, dust can be destroyed by SNe and reduce significantly its mass, and also it can grow by accretion of gas-phase metals in ISM. Thirdly, dust grains can be the formation sites of water, organic compounds, and amino acid closely related to the origin of life, and accordingly we can study the evolution of these interstellar matter essential for life by using our new simulations in future.

First we have described the details of the model and discussed the limitations and advantages of the model in investigating galaxy formation and evolution. We then have investigated the possible roles of dust in galaxy evolution by

using the new code and obtained some preliminary results. In particular, we have tried to grasp the possible roles of stellar radiation pressure on dust grains in the evolution of dust, gas-phase metals, and star formation histories (SFHs) of galaxies. The preliminary results that we have obtained in this study are briefly summarized as follows:

(1) The radiation pressure of stars on dust in disk galaxies can influence the time evolution of 3D dust distributions. Dust particles in a disk galaxy can be levitated from the initially thin disk and some fractions of dust can escape from the disk to locate outside the virial radius of its dark matter halo. This dynamical evolution of dust derived by stellar radiation strongly depends on the model parameters such as stellar ages (t_0), total dust extinction ($A_{\rm t}$), dust composition (e.g., silicate or graphite), and frequency-averaged radiation pressure coefficient ($Q^*_{\rm pr}$).

(2) The two basic roles of stellar radiation in the time evolution of 3D dust distributions are (i) thickening of the vertical structure of dust and (ii) flattening of the radial density profile. The above four parameters (e.g., $A_{\rm t}$) can determine the degrees of these thickening and flattening in the mass distributions of dust. For example, the models with higher $A_{\rm t}$ show a smaller degree of flattening in the dust distribution whereas those with younger disk ages (i.e., smaller t_0) show a larger degree of the flattening.

(3) Stellar radiation pressure can reduce the mass density of dust in a galactic disk so that it can also reduce the H_2 formation efficiency on dust grains. As a result of this, the star formation rate (SFR) can be severely reduced with the reduction level depending largely on $A_{\rm t}$. It should be noted, however, that this suppression of star formation by stellar radiation pressure is due to the adopted assumption that SFRs depend on the mass density of H_2 gas (not the total gas density) in the present study. Therefore, it is possible that the level of SF suppression by radiation pressure is overestimated in the present study.

(4) The inclusion of other dust-related physical processes, such as photo-electric heating and gas-dust heating, does not change the present results on the roles of stellar radiation pressure in galaxy evolution. It is found that photo-electric heating can suppress galaxy-wide star formation in the models with and without radiation pressure. Furthermore, gaseous drag of dust can lead to the slight enhancement of galactic SFRs, because the drag can prevent dust from escaping from thin galactic disks. We need to confirm these interesting effects of dust on galactic SFHs in our future studies by exploring a much wider parameter space for dust-related physical processes.

(5) One of the most important parameters for the evolution of dust and metal abundances is $f_{\rm dest}$, which is defined as the mass fraction of interstellar dust that is destroyed by SNe in a star-forming gas cloud. Although a possibly reasonable value of $f_{\rm dest}$ is ~ 0.01 in the present study, this parameter is yet to be constrained so well by observational and theoretical studies. Given its importance, it is our future study to determine the possible range of $f_{\rm dest}$ and its dependence on the physical properties of star-forming gas clouds.

(6) The present results suggest that although dust does not influence galaxy evolution so dramatically as SN and AGN feedback effects do, it can play significant roles in many aspects of galaxy formation and evolution. For example, the removal of metals through dust wind, suppression of H_2 formation due to dust removal, and photo-electric heating of gas by dust in ISM can influence chemical evolution, star formation histories, and stellar and gas dynamics in galaxies, respectively. These roles of dust in galaxy formation and evolution will need to be investigated extensively in future theoretical studies of galaxies for better understanding the formation and evolution processes of galaxies.

Thus the present new live dust particle method has enabled us to reveal the possible influences of dust-related physical processes on galaxy evolution. The dust properties of galaxies have been derived in the 'post-processing' of simulation data for almost all previous theoretical simulations of galaxy formation and evolution (e.g., derivation of dust mass from metal mass by assuming dust-to-metal ratios). The present study suggests that this 'post-processing' approach might not be realistic because dust itself can cause significant changes in galaxy evolution processes.

The present new model is still somewhat idealized (e.g., non-inclusion of dust size distributions in ISM) and therefore needs to be further improved so that we can properly investigate the physical properties of dust (e.g., evolving dust compositions and sizes) as well as their effects on galaxy formation and evolution, in particular, the evolution of galactic SEDs and molecular gas fraction. In our next paper, we will discuss how galaxy formation processes can be influenced by dust in a ΛCDM cosmology by using a more sophisticated live dust particle model.

6 ACKNOWLEDGMENT

I (Kenji Bekki; KB) am grateful to the referee for constructive and useful comments that improved this paper. Numerical simulations reported here were carried out on the three GPU clusters, Pleiades, Fornax, and gSTAR kindly made available by International Center for radio astronomy research(ICRAR) at The University of Western Australia, iVEC, and the Center for Astrophysics and Supercomputing in the Swinburne University, respectively. This research was supported by resources awarded under the Astronomy Australia Ltd' s ASTAC scheme on Swinburne with support from the Australian government. gSTAR is funded by Swinburne and the Australian Government's Education Investment Fund. KB acknowledges the financial support of the Australian Research Council throughout the course of this work.

REFERENCES

Aguirre, A., Hernquist, L., Schaye, J., Katz, N., Weinberg, D. H., Gardner, J., 2001, ApJ, 561, 521
Amblard, A., et al., 2010, A&A, 518, L9

Andrievsky, S. M., Luck, R. E., Martin, P., Lépine, J. R. D. 2004, A&A, 413, 159
Asano, R. S., Takeuchi, T. T., Hirashita, H., Nozawa, T., 2013, MNRAS, 432, 637
Athanassoula, E., 2003, MNRAS, 341, 1179
Bakes, E. L. O., Tielens, A. G. G. M., 1994, ApJ, 427, 822
Barsella, B., Ferrini, F., Greenberg, J. M., Aiello, S., 1989, A&A, 209, 349
Bekki, K., 2013, MNRAS, 432, 2298 (B13a)
Bekki, K., 2013, MNRAS, 436, 2254 (B13b)
Bekki, K., 2014, MNRAS, 444, 1615 (B14)
Bekki, K., 2015, accepted by ApJ (B15), arXiv1412.1239
Bekki, K., Shioya, Y., 1998, ApJ, 497, 108
Bekki, K., Shioya, Y., 2000, ApJ, 542, 201
Bekki, K., Shioya, Y., 2001, ApJS, 134, 241
Bekki, K., Couch, W. J., 2011, MNRAS, 415, 1783
Bekki, K., Tsujimoto, T., 2014, MNRAS, 444, 3879
Bianchi, S., Ferrara, A., 2005, MNRAS, 358, 379
Bron, E., Le Bourlot, J., Le Petit, F., 2014, A&A, 569, 100
Bruzual, G., Charlot, S., 2003, MNRAS, 344, 1000
Calura, F., Pipino, A., Matteucci, F., 2008, A&A, 484, 107
Calzetti, D., Armus, L., Bohlin, R. C., Kinney, A. L., Koornneef, J., Storchi-Bergmann, T., 2000, ApJ, 533, 682
Chiao, R. Y., & Wickramasinghe, N. C. 1972, MNRAS, 159, 361
Dale, D. A., Helou, G., Contursi, A., Silbermann, N. A., Kolhatkar, S., 2001, ApJ, 549, 215
Dekel, A., Silk, J., 1986, ApJ, 303, 39
Dekel, A., Birnboim, Y., 2006, MNRAS, 368, 2
De Rijcke, S., Schroyen, J., Vandenbroucke, B., Jachowicz, N., Decroos, J., Cloet-Osselaer, A., Koleva, M., 2013, MNRAS, 436, 2254
Di Matteo, T., Springel, V., Hernquist, L., 2005, Nature, 433, 604
Draine, B. T., 1978, ApJS, 36, 595
Draine, B. T., 2009, Physics of the interstellar and intergalactic medium
Dressler, A., 1980, ApJS, 42, 565
Dunne, L., Eales, S. A., 2001, MNRAS, 327, 697
Dwek, E., 1998, ApJ, 501, 643 (D98)
Edmunds, M., 2001, MNRAS, 328, 223
Eggen, O. J., Lynden-Bell, D., Sandage, A. R., 1962, ApJ, 136, 748
Ferrara, A., Ferrini, F., Barsella, B., Franco, J., 1991, ApJ, 381, 137 (F91)
Galametz, M., Madden, S. C., Galliano, F., Hony, S., Bendo, G. J., Sauvage, M., 2011, A&A, 532, 56
Galli, D., Palla, F., 1998, 335, 403
Gould, R. J., Salpeter, E. E., 1963, ApJ, 138, 393
Herbst, E., 2002, in Highlights of Astronomy, Vol. 12, Edited by H. Rickman. San Francisco, CA, Astronomical Society of the Pacific, p55
Herbst, E., van Dishoeck, E. F., 2009, ARA&A, 47, 427
Hernquist, L., & Katz, N., 1989, 70, 419
Hirashita, H., 1999, ApJ, 522, 220
Hirashita, H., 2012, MNRAS, 422, 1263
Hollenbach, D., Salpeter, E. E., 1971, ApJ, 163, 155
Hopkins, P. F., Quataert, E., Murray, N., MNRAS, 421, 3522
Inoue, A. K., 2003, PASJ, 55, 901
Jones, A. P., Tielens, A. G. G. M., Hollenbach, D. J., McKee, C. F., 1994, ApJ, 433, 797
Jonsson, P., 2006, MNRAS, 372, 2
Kennicutt, R. C., Jr., 1998, ApJ, 498, 541
Keres, D., Katz, N., Weinberg, D. H., Dave, R., 2005, MNRAS, 363, 2
Krumholz, M. R., McKee, C. F., Tumlinson, J., 2009, ApJ, 693, 216
Laibe, G., Price, D. J., 2014, MNRAS, 444, 1940
Larson, R. B., 1974, MNRAS, 169, 229
Larson, R. B., 2005, MNRAS, 359, 211
Lisenfeld, U., Ferrara, A., 1998, ApJ, 498, 145
Mannucci, F., Della Valle, M., Panagia, N., 2006, MNRAS, 370, 773
Ménard, B., Scranton, R., Fukugita, M., Richards, G., 2010, MNRAS, 405, 1025 (M10)
Mckee, C. F., 1989, in IAU Symp. 135, Interstellar Dust, Edited by Louis J. Allamandola and A. G. G. M. Tielens, p431
Navarro, J. F., Frenk, C. S., White, S. D. M., 1996, ApJ, 462, 563 (NFW)
Neto, A. F., 2007, MNRAS, 381, 1450
Noh, H., Vishniac, E. T., Cochran, W. D., 1991, ApJ, 383, 372
Noguchi, M., 1999, ApJ, 514, 77
Nozawa, T., Kozasa, T., Umeda, H., Maeda, K., Nomoto, K., 2003, ApJ, 598, 785
Pelupessy, F. I., Papadopoulos, P. P., van der Werf, P., 2006, ApJ, 645, 1024 (P06)
Popescu, C. C., Tuffs, R. J., 2013, MNRAS, 436, 1302
Predehl, P., Schmitt, J. H. M. M., 1995, A&A, 293, 889
Recchi, S., Kroupa, P., 2015, MNRAS, 446, 4168
Rowlands, K., et al. 2014, MNRAS, 441, 1040
Searle, L., Zinn, R., 1978, ApJ, 225, 357
Schmidt, M., 1959, ApJ, 129, 243
Schneider, R., Omukai, K., 2010, MNRAS, 402, 429
Sellwood, J. A.; Carlberg, R. G., 1984, ApJ, 282, 61
Shimonishi, T., Onaka, T., Kato, D., Sakon, I., Ita, Y., Kawamura, A., Kaneda, H., 2010, Interstellar Matter and Star Formation: A Multi-wavelength Perspective, ASI Conference Series, Vol. 1, pp 99, Edited by D. K. Ojha
Springel, V., Di Matteo, T., Hernquist, L., 2005, MNRAS, 361, 776
Sutherland, R. S., Dopita, M. A., 1993, ApJS, 88, 253
Tasker, E. J., 2011, ApJ, 730, 11
Theis, C., Orlova, N., 2004, A&A, 418, 959
Thompson, T. A., Quataert, E., Murray, N., 2005, ApJ, 630, 168
Tielens, A. G. G. M., 2005, The physics and chemistry of the interstellar medium, Cambridge University Press.
Tsujimoto, T., Nomoto, K., Yoshii, Y., Hashimoto, M., Yanagida, S., Thielemann, F.-K., 1995, MNRAS, 277, 945 (T95)
van den Hoek, L. B.; Groenewegen, M. A. T., 1997, A&AS, 123, 305 (VG97)
Watson, W. D., 1972, ApJ, 176, 103
White, S. D. M., Rees, M. J., 1978, MNRAS, 183, 341
Wolfire, M. G., McKee, C. F., Hollenbach, D., Tielens, A. G. G. M., 2003, ApJ, 587, 278
Xilouris, E., Alton, P., Alikakos, J., Xilouris, K., Boumis, P., & Goudis, C., 2006, ApJ, 651, L107
Zhukovska, S., Henning, T., 2013, A&A, 555, 99
Zubko, V., Dwek, E., Arendt, R. G., 2004, ApJS, 152, 211

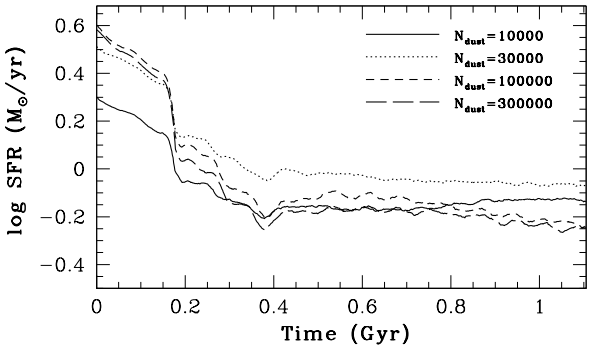

Figure A1. The star formation histories of the fiducial MW-type disk models with $N_{\rm dust}$ = 10000 (solid), 30000 (dotted), 100000 (short-dashed), and 300000 (long-dashed).

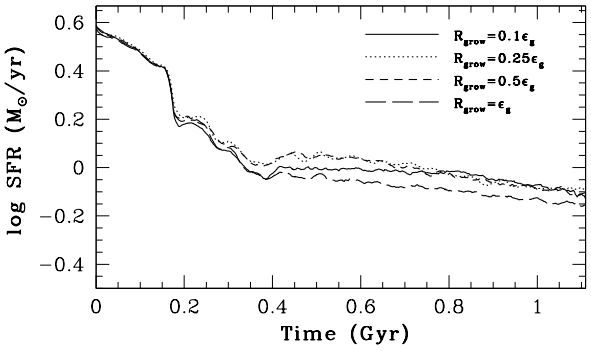

Figure B1. The star formation histories of the fiducial MW-type disk models $R_{\rm grow}$ = $0.1\epsilon_{\rm g}$ (solid), $0.25\epsilon_{\rm g}$ (dotted), $0.5\epsilon_{\rm g}$ (short-dashed), and $\epsilon_{\rm g}$ (long-dashed),

APPENDIX A: REQUIRED NUMBER OF DUST PARTICLES

In the present live dust particle method, the formation of H_2 is possible only on the surface of dust grains in galactic ISM. Accordingly, the time evolution of $f_{\rm H_2}$ and SFHs of galaxies depend on the dynamical evolution of dust. It is therefore possible that the present results on $f_{\rm H_2}$ evolution and SFHs of galaxies depend on the total number of dust particles ($N_{\rm dust}$) adopted in the present simulations. In order to investigate this important issue, we have run four comparative MW-type disk models without stellar radiation pressure and different $N_{\rm dust}$ and investigated whether the results depend on $N_{\rm dust}$.

Fig. A1 shows that the SFRs in MW-type disk galaxies do not depend strongly on $N_{\rm dust}$ as long as $N_{\rm dust} > 30000$ (30% of the total gas particle number). The model with $N_{\rm dust} = 10000$ appears to underestimate the SFR in the initial bursty star formation in the central region of the disk. It is confirmed that the final spatial distributions of dust does not depend strongly on $N_{\rm dust}$ either. This weak dependence on $N_{\rm dust}$ is very encouraging, because we do not have to adopt an excessively large number of dust particles to simulate the dust evolution of galaxies. Thus we conclude that the adopted number of $N_{\rm dust}$ is enough to investigate the possible roles of dust in galaxy evolution.

APPENDIX B: DEPENDENCE ON $R_{\rm GROW}$

Dust growth via accretion of gas-phase metals onto already existing dust grains and and dust destruction by SNe are both assumed to proceed locally depending on the physical conditions of ISM in the present study. In order to implement these processes, we have introduced a new parameter $R_{\rm grow}$ that defines the 'sphere of influence' within which the dust accretion and destruction rates are calculated for each dust particle based on the physical properties of gas around the dust particle. Since the present results can possibly depend strongly on this $R_{\rm grow}$, we need to investigate the possible dependence.

Fig. B1 clearly shows that galactic SFHs are qualitatively very similar between the MW-type disk models with four different $R_{\rm grow}$, though the SFRs at a given time step are slightly different between the four models. This is again encouraging, because we can estimate a reasonable $R_{\rm grow}$ from the adopted gravitational softening length (corresponding to the initial spatial resolution) of a simulation. However, this rather weak dependence on $R_{\rm grow}$ might be true only for the present galaxy evolution simulations for isolated disks. Thus, we need to confirm whether this is the case for other models such as galaxy formation models based on a ΛCDM cosmology.

APPENDIX C: A BRIEF SUMMARY OF THE NEW CHEMODYNAMICAL MODEL

Fig. C1 briefly summarizes the key elements of the new four-component chemodynamical model adopted in the present numerical study of galaxy evolution. The six key physical processes included in the code are (i) mixing of metals and dust ejected from SNe and AGB stars, (ii) dust formation from condensation of metals in stellar winds of SNe and AGB stars, (iii) dust growth through accretion of gas-phase metals onto already existing dust grains, (iv) dust destruction by SNe, (v) H_2 formation on dust grains from neutral hydrogen ('catalysis'), and (vi) consumption of gas and dust by star formation in molecular clouds in galaxies. The new model is quite different from previous standard three-component chemodynamical model in the sense that (i) dust-related physical processes are explicitly and self-consistently included and (ii) influences of dust evolution on chemical evolution of gas-phase metals is considered. The improved predictability of the new code is discussed extensively in the main text.

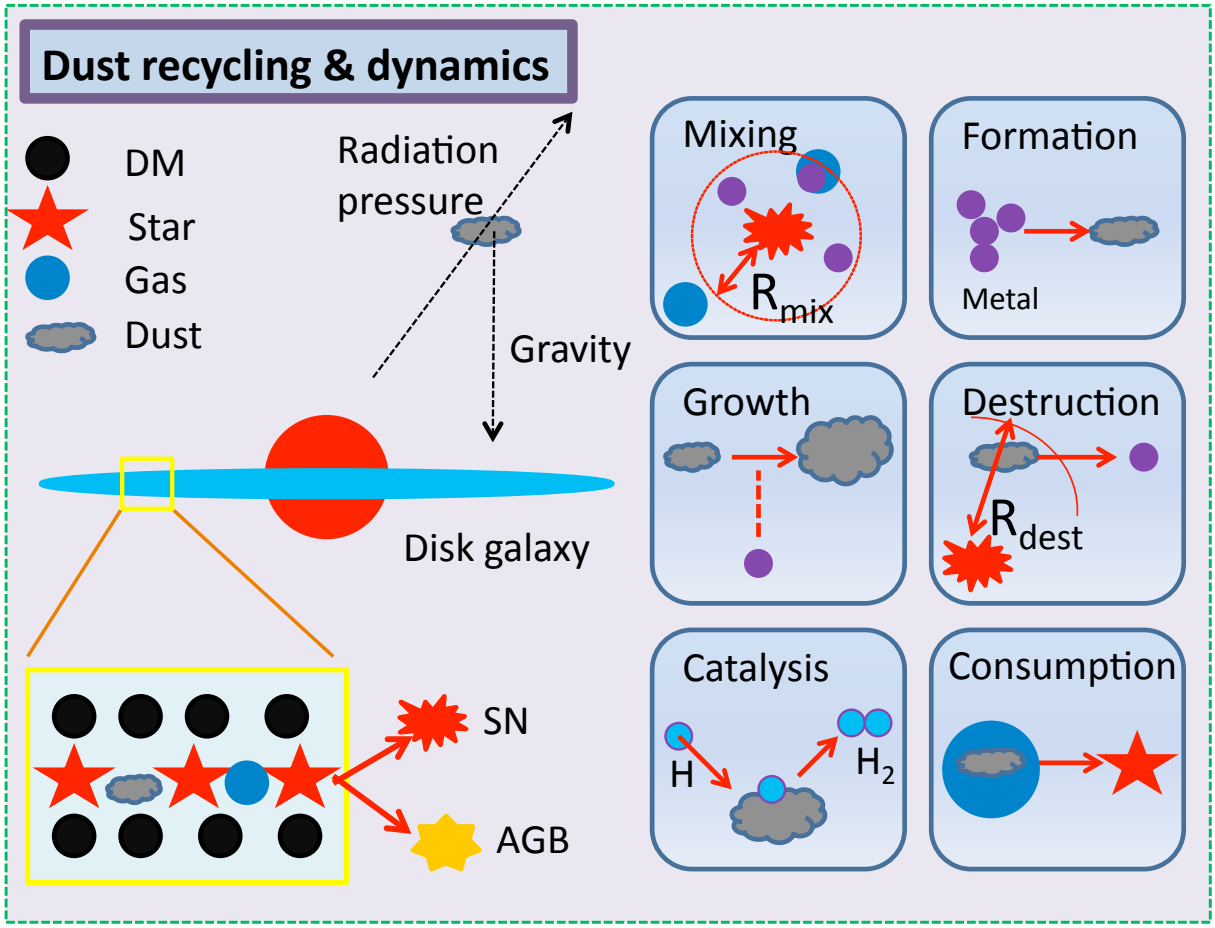

Figure C1. A cartoon representation of the new four-component chemodynamical model with live dust particles. A galaxy is composed of dark matter (DM), stars, gas, and dust, and the dust particles can move separately from gas in the new model. The six key dust-related physical processes, i.e., dust (metal) mixing, formation, growth, destruction, catalysis, and consumption are self-consistently included in the Nbody+hydrodynamical simulations of galaxies.